To appear in The Astronomical Journal, 2004 April
Preprint typeset using LaTeX style emulateapj v. 10/10/03

SLOAN DIGITAL SKY SURVEY SPECTROSCOPIC LENS SEARCH. I. DISCOVERY OF INTERMEDIATE-REDSHIFT STAR-FORMING GALAXIES BEHIND FOREGROUND LUMINOUS RED GALAXIES[1]

Adam S. Bolton[2], Scott Burles[2], David J. Schlegel[3], Daniel J. Eisenstein[4], and J. Brinkmann[5]

AJ, in press, 2004 April

ABSTRACT

We present a catalog of 49 spectroscopic strong gravitational lens candidates selected from a Sloan Digital Sky Survey sample of 50996 luminous red galaxies. Potentially lensed star-forming galaxies are detected through the presence of background oxygen and hydrogen nebular emission lines in the spectra of these massive foreground galaxies. This multiline selection eliminates the ambiguity of single-line identification and provides a very promising sample of candidate galaxy-galaxy lens systems at low to intermediate redshift, with foreground redshifts ranging from 0.16 to 0.49 and background redshifts from 0.25 to 0.81. Any lenses confirmed within our sample would be important new probes of early-type galaxy mass distributions, providing complementary constraints to those obtained from currently known lensed high-redshift quasars.

Subject headings: gravitational lensing—galaxies: elliptical and lenticular, cD—galaxies: starburst

1. INTRODUCTION AND MOTIVATION

In its strongest form, gravitational lensing produces unmistakably distorted, amplified, and multiplied images of distant astronomical objects. It is therefore not surprising that the majority of known galaxy-scale gravitational lens systems have been discovered through imaging observations. However, a small number of lenses have been discovered spectroscopically, with the spectrum of a targeted galaxy showing evidence of emission from a background source and follow-up imaging revealing lensing morphology. The three most secure examples are the lensed quasars 2237+0305 (Huchra et al. 1985) and SDSS J0903+5028 (Johnston et al. 2003) and the lensed Lyman-α emitting galaxy 0047−2808 (Warren et al. 1996, 1998, 1999). Several authors have made predictions for the frequency of lensed quasar discoveries in galaxy redshift surveys (Kochanek 1992; Mortlock & Webster 2000, 2001). Others, inspired by the discovery of 0047−2808, have undertaken spectroscopic searches for lensed Lyman-α-bright galaxies (Hewett et al. 2000; Willis et al. 2000; Hall et al. 2000; Burles et al. 2000). The idea behind such searches is that a massive foreground galaxy should act as an effective gravitational lens of *any* object positioned sufficiently far behind it and at small enough impact parameter, and any emission features from such lensed objects should be detectable in the spectra of the foreground galaxy. Therefore a search for discrepant emission features in galaxy spectra can potentially lead to a sample of gravitational lens systems that would not be discovered in broadband imaging searches due to faintness of source relative to lens. This "lenses-looking-for-sources" approach is complementary to lens searches such as the recently completed Cosmic Lens All-Sky Survey (CLASS; Myers et al. 2003; Brown et al. 2003) which proceed by targeting sources and looking for evidence of an intervening lens.

With its massive scale and quality of data, the spectroscopic component of the Sloan Digital Sky Survey (SDSS) provides an unprecedented opportunity for spectroscopic galaxy-galaxy gravitational lens discovery. This paper presents the first results of such a search within a sample of ∼51,000 SDSS Luminous Red Galaxy (LRG) spectra (Eisenstein et al. 2001, hereafter E01): a catalog of candidate lensed star-forming galaxies at intermediate redshift. The lens candidates presented in this paper were detected by the presence of not one but (at least) three emission lines in the LRG spectra identified as nebular emission from a single background redshift: [O II] $\lambda\lambda$3728 and two out of the three of Hβ λ4863, [O III] λ4960, and [O III] λ5008 (all emission-line wavelengths in this paper are vacuum values, in Angstroms). This implies a maximum redshift of $z \sim 0.8$ for any candidate lensed galaxies: at higher redshifts, [O III] emission moves off the red end of the SDSS spectrograph.

The lensing cross section of a particular foreground galaxy is lower for intermediate-redshift sources than high-redshift sources, and in this sense the lens search we describe here is at a disadvantage relative to searches for lensed high-redshift Lyman-α emitters. However, the identities of the emission lines in the sample we present here are absolutely unambiguous. This cannot be said for spectroscopic Lyman-α lens candidates, which are typically detected as single discrepant emission lines and are difficult to distinguish from lower-redshift emission or (in the case of a huge survey such as the SDSS) non-astrophysical spectral artifacts. (A forthcoming paper will present SDSS single-line [O II] and Lyman-α lens candidates.) Our spectroscopic lens search based on multiple-line detection has further advantages. First, the source redshift of any lensed galaxies will be known from the outset. Second, for a given limiting line flux, star-forming galaxies at intermediate redshift

[1] Based in part on observations obtained with the 6.5-m Clay telescope of the Magellan Consortium.

[2] Department of Physics and Center for Space Research, Massachusetts Institute of Technology, 77 Massachusetts Avenue, Cambridge, MA 02139 (bolton@mit.edu, burles@mit.edu)

[3] Princeton University Observatory, Princeton, NJ 08544-1001 (schlegel@astro.princeton.edu)

[4] Steward Observatory, University of Arizona, 933 North Cherry Avenue, Tucson, AZ 85721

[5] Apache Point Observatory, P.O. Box 59, Sunspot, NM 88349

are more numerous on the sky than Lyman-α emitters at high redshift (see Hippelein et al. 2003; Maier et al. 2003), and hence strong lensing events could be more frequent despite decreased lensing cross sections. The non-lensed source population should thus be more amenable to study and characterization (Hogg et al. 1998, for example), facilitating lens statistical analysis. Finally, intermediate-redshift lensed galaxies would probe the mass distribution of the lens population in a systematically different manner than do high-redshift sources.

The search for new lens systems is motivated by the unique power of gravitational lensing to constrain the mass distribution of the lensing galaxy. Miralda-Escudé & Lehár (1992) argued that strong galaxy-galaxy gravitational lenses in the optical band should be both ubiquitous and of great scientific interest, but their detection has proved difficult. In addition to the optical Einstein ring 0047−2808 mentioned above, Hewett et al. (2000) have published one more spectroscopic galaxy-lens candidate. *Hubble Space Telescope* (*HST*) imaging has also had some success in detecting lensed galaxies, as described by Crampton et al. (2002), Ratnatunga, Griffiths, & Ostrander (1999), and Fassnacht et al (2003), but spectroscopic confirmation remains a challenge in most cases. Lensed galaxies are especially useful for investigating the mass distribution of the lensing galaxy because unlike lensed quasars they are spatially resolved sources which provide more detailed constraints (Kochanek & Narayan 1992, for example). As with lensed quasars, the relative angular deflections between multiple images can constrain the total deflecting lens mass. But the relative distortions of multiple images can provide constraints as well, probing the slope of the radial mass profile and allowing more detailed connection with theories of galaxy formation and Cold Dark Matter (CDM). The promise of our candidate sample is enhanced by the fact that lens *and* source redshifts for any confirmed lens systems will be known from the outset with great precision; this is generally not the case for lenses discovered in optical imaging or radio data.

The lack of sufficient lensing constraints on the radial slope of the galaxy mass profile in lensed quasar systems is the greatest source of uncertainty in the Hubble constant (H_0) values derived from the time delays between images (Schechter 2004), which remain systematically low compared to the current best H_0 values from the distance ladder (Freedman et al. 2001) and cosmic microwave background (Spergel et al. 2003); Kochanek (2002a,b, 2003) highlights the importance of resolving this discrepancy. Any galaxy-galaxy lenses confirmed within our current list of candidates would help to solve this problem by expanding the sample for ensemble lensing studies of early-type galaxy mass profiles like that of Rusin, Kochanek, & Keeton (2003b) and allowing for the inclusion of distortion information as mentioned above. The generally lower lens and source redshifts of our candidate systems as compared to known lens systems are also of particular interest because the images of any strong lenses within our sample will tend to form at smaller *physical* radii within the lens galaxy than in current lens systems (see Rusin et al. 2003a, Table 1), thus probing elliptical galaxy mass profiles in a systematically different manner[6]. A large enough sample of strongly lensed star-forming galaxies could even be monitored directly for supernovae. Multiple images of the same supernova would give time delays and H_0 measurements, as numerous authors have envisioned (Refsdal 1964; Porciani & Madau 2000; Holz 2001; Goobar et al. 2002; Oguri & Kawano 2003). If we assume one supernova per galaxy per century as an order-of-magnitude estimate (Doggett & Branch 1985), a program to monitor ~ 50 lensed galaxies for several years would have a good chance of success.

Numerous studies have addressed the inability of standard macroscopic galaxy mass models to predict the flux ratios observed between images of strongly lensed quasars. Some authors have suggested that this phenomenon may be due to the effects of substructure in the lensing galaxy on the scale of either CDM sub-halos (Mao & Schneider 1998; Metcalf & Madau 2001; Chiba 2002; Dalal & Kochanek 2002) or stars (Witt, Mao, & Schechter 1995; Schechter & Wambsganss 2002), while others have invoked macroscopically modified lens models as a possible explanation (Evans & Witt 2003; Möller, Hewett, & Blain 2003). A sizeable sample of strongly lensed galaxies would provide valuable insight into this problem: by virtue of the arcsecond-scale intrinsic angular size of the source, galaxy-galaxy lenses will be immune to the lensing effects of any substructure with lensing deflection angles on the scale of microarcseconds (stars) or milliarcseconds (sub-halos). If the suppressed saddle point image fluxes seen in many quasar lenses are indeed due to macroscopic inadequacies in the standard lens models, similar effects should be seen in galaxy-galaxy lenses. If on the other hand these effects are due to micro/millilensing by substructure, they should be absent from lensed galaxy systems.

2. SEARCH SAMPLE

The Sloan Digital Sky Survey is a project to image roughly one-quarter of the sky in five optical bands and obtain spectroscopic follow-up observations of $\sim 10^6$ galaxies and 10^5 quasars. York et al. (2000) provide a technical summary of the survey, Gunn et al. (1998) describe the SDSS camera, Fukugita et al. (1996), Hogg et al. (2001), and Smith et al. (2002) discuss the photometric system and calibration, Pier et al. (2003) discuss SDSS astrometry, Blanton et al. (2003) present the spectroscopic plate tiling algorithm, and Stoughton et al. (2002) and Abazajian et al. (2003) describe the survey data products. Approximately 12% of the galaxy spectroscopic fibers are allocated to the LRG sample (E01), selected to consist of very luminous ($\gtrsim 3L_\star$)—and hence massive—early-type galaxies at higher redshift than the galaxies of the main sample (Strauss et al. 2002). We expect these LRGs to be particularly effective gravitational lenses of any objects positioned suitably behind them, and we concentrate our spectroscopic lens search on them. We also note that LRGs should have little dust and therefore any lensed background galaxies should suffer minimal extinction.

[6] The lowest-redshift lensed quasar currently known, RXJ 1131−1231, has $z = 0.658$ (Sluse et al. 2003).

The sample for our current study consists of 50996 spectra taken between 5 March 2000 and 27 May 2003 of SDSS imaging objects flagged as `GALAXY_RED` by the photometric pipeline (Lupton et al. 2001) for passing either of the LRG cuts described by E01, reduced by the SDSS spectroscopic pipeline (J. Frieman et al., in preparation), and selected to have redshifts between 0.15 and 0.65 as determined by the `specBS` redshift-finding software (D. J. Schlegel et al., in preparation). The low-redshift cutoff is needed because less massive galaxies start to pass the photometric cuts below $z \lesssim 0.15$ and pollute the volume-limited LRG sample; see the discussion in E01 and the bimodal LRG sample redshift histogram in Stoughton et al. (2002, Fig. 14).

In addition to being much more massive than the average galaxy, LRGs have another property that makes them well suited to a spectroscopic lens survey: their spectra are extremely regular and well-characterized (see Eisenstein et al. 2003). To determine the spectroscopic redshift of an SDSS target galaxy with observed specific flux f_λ and one-sigma sky+source noise spectrum σ_λ, the `specBS` program employs a small set of galaxy eigenspectra (four in the reductions for this study) derived from a rest-frame principal-component analysis (PCA) of 480 galaxy spectra taken on SDSS plate 306, MJD 51690. This eigenbasis is incrementally redshifted, and a model spectrum is generated from the best-fit linear combination to the observed spectrum at each trial redshift, with the final redshift assignment given by the trial value that yields the overall minimum χ^2. Although redshift is the primary output of this procedure, a byproduct of `specBS` is the best-fit model spectrum itself, $\widetilde{f}_\lambda$. In the case of LRGs, $\widetilde{f}_\lambda$ typically provides a very detailed and accurate fit to f_λ, with a reduced χ^2 of order unity over almost 4000 spectral pixels (roughly 1600 spectral resolution elements) attained with only 8 free parameters: a redshift, the four eigen-galaxy coefficients, and the three terms of a quadratic polynomial to fit out spectrophotometric errors and extinction effects, both of which exist at the few-percent level[7]. This extremely regular spectral behavior allows us to form residual LRG spectra

$$f_\lambda^{(r)} \equiv f_\lambda - \widetilde{f}_\lambda \tag{1}$$

that are in principle realizations of σ_λ. Nebular emission lines from galaxies along the line of sight other than the target LRG will not be modeled by `specBS` and should appear as significant features localized in wavelength within these residual spectra. Figure 1 shows the median 1-σ line flux sensitivity within our LRG residual spectrum sample as a function of wavelength. The (20th, 50th, 80th)-percentile LRG spectra themselves have a median signal-to-noise per pixel of (3.3, 5.1, 9.6) at the SDSS resolution of $\lambda/\Delta\lambda \approx 1800$.

3. CANDIDATE SELECTION

This section describes our candidate selection routine in detail. Briefly stated, we select as initial candidates those spectra that show *both* blended [O II] $\lambda\lambda$3728 at $S/N > 3$ *and* two out of the three lines Hβ λ4863, [O III] λ4960, and [O III] λ5008 at $S/N > 2.5$, then cull the candidate list by applying cuts based on more detailed fits to the presumed emission features, and finally remove any obviously spurious detections. This selection process yields a substantial number of promising systems without an excess of obvious false positives.

[7] The `specBS` outputs for the SDSS-DR1 sample are available from the website `http://spectro.princeton.edu`.

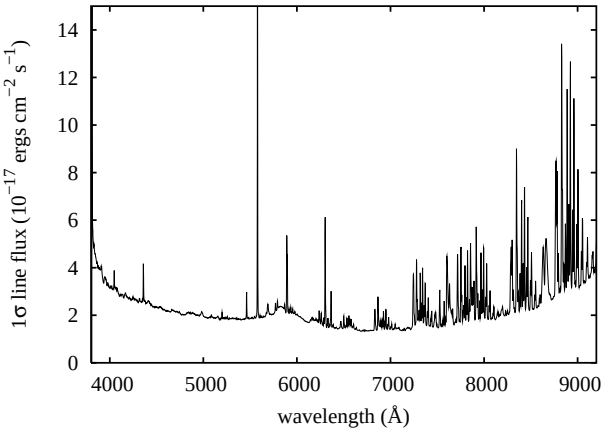

FIG. 1.— LRG sample median line-flux noise spectrum. Shown is the 1-σ noise on best-fit line fluxes for optimal extraction of Gaussian-shaped residual emission features with spectral width σ =1.2-pixel ($\simeq$ 83 km s^{-1}). Reported pixel flux variances have been rescaled as described in Appendix A prior to the calculation of this noise spectrum.

3.1. *Initial Emission Feature Detection*

The key element in the first step of our lens candidate selection (described fully in § 3.2 below) is a straightforward matched-filtering procedure to search for significant emission features by fitting a Gaussian line profile at each point in the residual spectrum (Pratt 1978; Hewett et al. 1985). We describe our implementation here so as to be explicit. Let $f_j^{(r)}$ be the residual flux in pixel j and σ_j^2 be the statistical variance of $f_j^{(r)}$ [8]. Also let $\{u_i\}$ describe a Gaussian kernel, centered on $i = 0$, with i running from $-i_{\rm lim}$ to $i_{\rm lim}$, and normalized such that $\sum_i u_i = 1$. The maximum-likelihood estimator $\bar{A}_j$ for the line flux A_j of any $\{u_i\}$-shaped residual emission feature centered on pixel j is that which minimizes

$$\chi_j^2 = \sum_{i=-i_{\rm lim}}^{i_{\rm lim}} \left(A_j u_i - f_{(j+i)}^{(r)} \right)^2 \Big/ \sigma_{(j+i)}^2 \quad . \tag{2}$$

Differentiating (2) with respect to A_j, setting the resulting expression to zero, and solving yields

$$\bar{A}_j = C_j^{(1)} \Big/ C_j^{(2)} \quad , \tag{3}$$

where we have defined the convolutions

$$C_j^{(1)} \equiv \sum_i f_{(j+i)}^{(r)} u_i / \sigma_{(j+i)}^2 \quad , \tag{4}$$

$$C_j^{(2)} \equiv \sum_i u_i^2 / \sigma_{(j+i)}^2 \quad . \tag{5}$$

[8] Conversion from units of ergs cm^{-2} s^{-1} Å^{-1} to units of ergs cm^{-2} s^{-1} pixel^{-1} is made using the re-binned SDSS spectroscopic pixel scale relation $d\lambda = \lambda \times 10^{-4} \ln(10)\, d(\text{pixels})$.

The variance of $\bar{A}_j$ (under the assumption of uncorrelated Gaussian errors in $f_j^{(r)}$ as described by σ_j^2) is given by

$$\sigma^2_{\bar{A},j} = 1 \Big/ C_j^{(2)} \quad . \tag{6}$$

The signal-to-noise ratio for a fitted Gaussian profile centered on pixel j is therefore

$$(S/N)_j = C_j^{(1)} \Big/ \sqrt{C_j^{(2)}} \quad . \tag{7}$$

Our null hypothesis is an absence of emission features in the residual spectra that should manifest as the $\{(S/N)_j\}$ being Gaussian-distributed about zero with unit variance: this should hold at most wavelengths in most spectra. We approach the initial search for emission lines in the residual spectra as a search for significance peaks with (S/N) greater than some threshold value. Although insensitive to goodness-of-fit, this convolution-based detection scheme executes quickly and is therefore well suited to the initial search for residual emission features within our large spectral sample. Appendix A describes a noise-rescaling process that we employ to control the incidence of false-positive emission-feature detections (due primarily to imperfect sky subtraction) without masking regions of the spectrum.

3.2. *Multi-Line Background Systems: Detection, Fitting, and Rejection*

Multiple emission features at the same redshift will have redshift-independent wavelength ratios. The fully reduced SDSS spectra have been re-binned at a constant-velocity pixel scale of 69 km s^{-1}, giving a redshift-independent pixel offset between features. Our operational scheme is thus to search for coincident (S/N) peaks between multiple copies of a single filtered residual spectrum that have been shifted relative to one another. For [O II] $\lambda\lambda$3728 detection, we filter each residual spectrum with a $\sigma = 2.4$-pixel Gaussian kernel (matched to the typical width of blended [O II] $\lambda\lambda$3728 emission seen in SDSS starburst galaxies). We take copies of the same residual spectrum "blueshifted" by integer pixel amounts so as to place Hδ λ4103, Hγ λ4342, Hβ λ4863, [O III] λ4960, [O III] λ5008, [N II] λ6550, Hα λ6565, [N II] λ6585, [S II] λ6718, and [S II] λ6733 as close as possible to 3728.48 Å, the geometric-mean wavelength of the [O II] $\lambda\lambda$3728 doublet. These shifted spectra are filtered with a $\sigma = 1.2$-pixel Gaussian kernel (matched to the typical width of SDSS starburst [O III] λ5008 emission), with the sub-pixel part of the line offset relative to 3728.48 Å incorporated by offsetting the kernel. Any pixel in the filtered S/N spectra with value greater than 3 for [O II] $\lambda\lambda$3728 and value greater than 2.5 for two out of Hβ λ4863, [O III] λ4960, and [O III] λ5008 is tagged as a "hit". A group of adjacent "hit" pixels is reduced to the single pixel with the greatest quadrature-sum S/N for lines detected above the threshold (in effect, the pixel most inconsistent with the null hypothesis). Spectra with more than one isolated hit are rejected. The spectra are only searched in regions that would correspond to emission from $\gtrsim 5000$ km s^{-1} behind the targeted LRG.

The preceding selection leads to 163 hits within our 51,000 spectra. For each hit, we explore a grid of redshift and intrinsic emission-line-width values for the background galaxy to find a best-fit model. At each grid point we fit a Gaussian profile to any emission line initially detected above a 2.0-S/N threshold, with the line center determined by the trial redshift and line-width given by the quadrature sum of the trial intrinsic line-width and the measured spectrograph resolution at the observed wavelength of each line. [O II] $\lambda\lambda$3728 is fit with a double Gaussian profile. We adopt as best values for background redshift z_{BG} and (Gaussian-σ) intrinsic line-width σ_e those that give the minimum χ^2 over all detected lines. The z_{BG} extent of our grid corresponds to ± 2 pixels, and the explored σ_e range runs from 0 to 2 pixels (0 to 138 km s^{-1}).

Following these fits, we subject the candidate sample to several cuts. First, we reject any system where no convergent (minimum χ^2) value for z_{BG} is found within the explored ± 2-pixel range: real background emission systems should have convergent best-fit redshifts roughly coincident with their convolution-based S/N peaks. Similarly, we cut systems with no convergent σ_e between 0 and 2 pixels: the features of real systems should neither be narrower than the spectrograph resolution nor wider than a reasonable upper limit for emission features of faint star-forming galaxies. Finally, we compute a total signal-to-noise ratio for the fit, defined as the total best-fit flux in [O II] $\lambda\lambda$3728 and all other lines initially detected at $S/N \geq 2.5$ divided by the quadrature-sum of the 1-σ noise from those line fits, and impose a cut in the total-S/N–χ^2_r plane (χ^2_r being the χ^2 per degree of freedom in the fit). We cut any system with a total S/N less than the greater of 6 and $6 + 3(\chi^2_r - 1)$. This removes both low-S/N candidates and candidates whose χ^2_r values are too high to be explained by high-S/N emission features showing significant non-Gaussian structure. (These cuts were designed to be a quantitative expression of our own judgements about which candidate systems look real upon spectrum inspection and which do not; the justifications are somewhat *a posteriori*.) This cutting procedure reduces the 163 hits to 61 candidate systems. Finally, we prune 12 candidates from the list that survive the automated culling but are clearly explained by either over-fit LRG stellar absorption, under-modeled LRG line emission, exceptionally poor data quality, or a generally flawed template fit, leaving the 49 good candidate systems that we present.

This search for background galaxy emission lines digs rather deep into the noise of our spectroscopic sample. To gauge the incidence of false positives in our final candidate list, we make a parallel run of the detection, fitting, and automated rejection procedure with the following rest-wavelength perturbations: Hβ λ4863 $\rightarrow$ 4833, [O III] λ4960 $\rightarrow$ 4945, and [O III] λ5008 $\rightarrow$ 5023. These perturbations alter all of the redshift-independent wavelength ratios among these lines and between all of them and [O II] $\lambda\lambda$3728; this modified detection procedure no longer selects for real multi-line emission, but only for noise features. The "false candidates" that result from this perturbed procedure are randomly shuffled along with the candidates from the original procedure, and all are examined together when making the final pruning judgements. The perturbed procedure yields 88 hits and 7 post-cut candidates; all 7 are pruned upon inspection without knowledge of their intrinsic falseness. This im-

plies that the vast majority of our candidates are indeed background galaxies and not simply noise features.

4. CANDIDATE SYSTEMS

4.1. *Catalog*

In this section we present our catalog of 49 candidate lensed star-forming galaxies selected to have [O II] $\lambda\lambda$3728 emission at S/N of 3 or higher and emission from two out of the three of Hβ λ4863, [O III] λ4960, and [O III] λ5008 each at S/N of 2.5 or higher, at a redshift significantly greater than that of the primary target LRG. Table 1 lists various properties of the candidate lens systems. LRG r de Vaucouleurs model magnitudes are determined from SDSS imaging and photometric reduction. LRG redshifts and velocity dispersions are as provided by `specBS`; the software fits for velocity dispersions σ_v using a set of 24 stellar eigenspectra derived from a PCA of the ELODIE spectral library (Prugniel & Soubiran 2001). We report all σ_v values from the database, although some are likely unreliable; see the notes of Table 1. We also report emission-line redshifts of the detected background galaxies. Using the observed LRG and background redshifts and the observed LRG σ_v, and assuming a singular isothermal sphere (SIS) LRG luminous+dark matter distribution, we calculate a "best guess" for the angular scale of any lensing that might be present in these systems as $\Delta\theta = 8\pi(\sigma_v^2/c^2)(D_{LS}/D_S)$. ($D_{LS}$ and D_S are angular-diameter distances from lens to source and from observer to source[9]). This is the separation between the two images of a strongly lensed object in the SIS model; it is also the radius of the strong-lensing region of the image plane, and twice the radius of ring images of compact sources directly behind the lens (Narayan & Bartelmann 1996, for example). Finally, for each candidate system we report the detected background [O II] $\lambda\lambda$3728 line flux from the best-fit double Gaussian profile, a list of other lines detected at $S/N > 2.5$, and the total S/N of the background galaxy emission-line fit as defined in § 3.2. The reported background line fluxes should be viewed with suspicion: the spatial alignments of the background galaxies are unknown, and the spectroscopic fibers will not necessarily have captured all of their light. In addition, most of the reduced candidate LRG spectra have been rescaled based on smear exposures that attempt to account for LRG flux falling outside the 3″ fiber (Stoughton et al. 2002); we have removed this correction from the tabulated line fluxes, as it has no physical relation to the background emission-line galaxies. Figure 2 shows the SDSS discovery spectra and best-fit model spectra, along with close-up views of the residual (data − model) spectra in the wavelength ranges corresponding to redshifted background [O II] $\lambda\lambda$3728, Hβ λ4863, [O III] λ4960, and [O III] λ5008. Smear corrections have not been removed from these plots.

Although we detect line emission clearly, evidence of background galaxy *continuum* in the residual spectra of our candidate systems is scarce. This is not surprising, for three reasons. One, the LRG sample was selected for particular broadband color and luminosity, and significant background continuum would likely perturb an LRG out of the sample. Two, any faint background continuum present in an LRG spectrum will largely project onto the LRG-redshift eigenspectrum set and low-order polynomial fit used by `specBS`, and will be subtracted along with the LRG model when forming the residual spectrum. Three, these background galaxies are likely to be high-equivalent-width star-forming systems, and since their line fluxes are detected just above the noise threshold, the associated continuum will typically be lost in the noise. Nevertheless, we may obtain a higher signal-to-noise picture of the background galaxies that we detect by constructing a median spectrum as follows. First we transform the residual spectra of our candidate systems into units of erg cm^{-2} s^{-1} pixel^{-1}, which is a redshift-independent quantity since the SDSS pixels are of constant velocity width. We then shift these residual spectra into the rest frame of the background galaxy, rounded to the nearest whole pixel, and transform back to erg cm^{-2} s^{-1} Å^{-1}. Next we renormalize the spectra by dividing each one by its best-fit [O II] $\lambda\lambda$3728-flux value. We then take the median value at each pixel, and restore physical normalization by multiplying this median spectrum by the sample-median best-fit [O II] $\lambda\lambda$3728-flux value. The resulting median spectrum is shown in Figure 3. Although there is no discernible continuum in the individual residual spectra, we can see a 4000-Å continuum break in the median spectrum; we also see Hγ, Hα, [N II] and [S II] emission lines in addition to the lines for which we select. This gives further evidence that we have successfully detected and identified background emission features.

4.2. *Lenses or Not?*

We have with certainty detected emission from galaxies behind foreground LRGs. For a system to be a strong gravitational lens, the background galaxy must be located at sufficiently small impact parameter relative to the LRG center. The true incidence of lensing within our sample can best be determined and studied with either narrow-band imaging or integral-field spectroscopy. Such observations could spectrally isolate the background line flux and resolve it spatially to reveal any lensing morphology. SDSS broadband imaging offers some hope for answering the lensing question, but in general Sloan images do not detect late-type galaxies at redshift $z \sim 0.5$ at very high S/N. Figure 4 shows 40″ × 40″ SDSS r postage-stamp images centered on the candidate systems, with linear gray-scaling from -3-σ sky noise to peak LRG surface brightness. Evidence of significantly offset neighboring broadband emission is seen in some images, but it would be difficult to rule out many systems as definite non-lenses based on SDSS-quality images. In the spirit of a purely spectroscopic survey, we present as candidates all systems selected spectroscopically. Furthermore, we note that many of these LRGs live in high-density group/cluster environments, and neighboring images may be at the LRG redshift and not the source of the background emission that we detect.

In preparation for integral-field spectroscopic follow-up, we have obtained broadband reconnaissance images of 14 of our candidate systems (as indicated in Table 1) using the Magellan consortium's 6.5-m Clay telescope at Las Campanas Observatory. These short g- and i-

[9] Throughout this paper, we assume a cosmology of $(\Omega_M, \Omega_\Lambda) = (0.3, 0.7)$ and a Hubble constant H_0 of 70 km s^{-1} Mpc^{-1}. Since $\Delta\theta$ is proportional to a distance ratio, it is independent of H_0.

Table 1. Properties of Candidate Lens Systems

System Name[a]	Plate-MJD -Fiber	In DR1?	r (de Vauc.)	z (LRG)	σ_v (km s^{-1})	z (BG)	$\Delta\theta$[b] ($''$)	[O II] $\lambda\lambda$ Flux[c]	Other Lines[d]	Total S/N
SDSS J002431.96+003123.1[e]	0390-51900-589	Y	18.48±0.02	0.3979	286±19[f]	0.5952	1.39	20 ± 2	d,e	11.6
SDSS J003524.12+002400.2[e]	0689-52262-632	N	17.88±0.01	0.2017	176±21	0.2708	0.43	19 ± 3	c,e,g,h,i	10.8
SDSS J003753.21−094220.1[e]	0655-52162-392	Y	16.79±0.01	0.1955	279±10	0.6322	2.94	23 ± 4	a,c,d,e	16.0
SDSS J010933.73+150032.4[e]	0422-51811-508	Y	18.26±0.01	0.2939	251±19[f]	0.5248	1.47	19 ± 3	c,d,e	10.2
SDSS J011123.49+000012.7	0694-52209-076	N	19.18±0.03	0.4516	86±25[f]	0.5011	0.04	19 ± 2	c,e	11.6
SDSS J021652.53−081345.4[e]	0668-52162-428	Y	17.33±0.01	0.3317	333±23[f]	0.5235	2.13	25 ± 4	c,d	8.7
SDSS J032454.50−011029.1[e]	0414-51869-244	Y[g]	18.85±0.03	0.4453	267±35[f]	0.6240	1.03	22 ± 2	b,c,d,e	16.5
SDSS J073728.44+321618.6	0541-51959-145	N	17.85±0.01	0.3223	338±16	0.5812	2.67	62 ± 5	a,b,c,d,e	24.7
SDSS J080532.29+303712.7	0860-52319-452	N	17.95±0.01	0.3200	334±17	0.3809	0.94	54 ± 4	c,e,g,h	17.0
SDSS J085038.70+020155.2	0468-51912-362	Y	18.70±0.02	0.4114	251±41[f]	0.5672	0.88	12 ± 4	d,e	6.2
SDSS J091205.31+002901.1	0472-51955-429	Y	16.08±0.01	0.1642	326±12	0.3240	2.90	26 ± 4	b,c,e,g	11.5
SDSS J092857.33+440059.1	0870-52325-465	N	17.76±0.01	0.2908	198±24[f]	0.4538	0.75	29 ± 4	d,e	9.4
SDSS J093543.93−000334.8	0476-52314-177	N	17.52±0.01	0.3475	396±35[f]	0.4670	2.10	15 ± 3	c,e	8.8
SDSS J095629.78+510006.3	0902-52409-068	N	16.84±0.01	0.2405	334±15	0.4700	2.94	31 ± 3	c,e	11.5
SDSS J101051.52+060432.6	0996-52641-106	N	17.99±0.01	0.3475	183±22[f]	0.4797	0.48	18 ± 3	c,e	7.9
SDSS J102551.32−003517.4	0272-51941-151	Y	16.10±0.01	0.1589	264±11	0.2764	1.64	18 ± 3	d,e,g,i	14.6
SDSS J102927.54+611505.0	0772-52375-140	N	16.12±0.01	0.1574	228±14	0.2512	1.08	31 ± 5	c,e,f,g,h,i	18.7
SDSS J110102.15+073622.0	1002-52646-504	N	17.27±0.01	0.2058	217±17[f]	0.5809	1.65	52 ± 11	c,e	6.1
SDSS J112837.77+583526.8	0951-52398-036	N	18.19±0.01	0.3809	223±28[f]	0.5466	0.78	29 ± 4	c,d,e	11.2
SDSS J113629.47−022303.9	0328-52282-350	N	18.84±0.02	0.3936	321±27[f]	0.4646	0.81	9 ± 3	c,d,e	8.9
SDSS J115107.04+645540.3	0598-52316-477	N	18.29±0.01	0.3804	260±27[f]	0.5435	1.05	14 ± 3	c,e	6.5
SDSS J115510.09+623722.1	0777-52320-501	N	18.04±0.02	0.3751	303±34[f]	0.6690	2.08	16 ± 4	d,e	7.5
SDSS J123851.61+670928.1	0494-51915-074	Y	17.10±0.01	0.2312	238±10	0.4446	1.47	16 ± 2	c,e	10.5
SDSS J125919.07+613408.3	0783-52325-279	N	17.33±0.01	0.2334	253±16	0.4488	1.67	23 ± 3	c,e	10.6
SDSS J130035.91+652235.9	0602-52072-332	Y	18.40±0.01	0.3050	300±24[f]	0.3300	0.36	16 ± 3	c,e,g,j	12.0
SDSS J131047.95+621154.7	0784-52327-350	N	16.68±0.01	0.1984	226±12	0.5141	1.71	16 ± 5	c,e	6.6
SDSS J133828.80−004915.2	0298-51955-001	Y	18.02±0.02	0.3496	111±12[f]	0.4425	0.14	18 ± 3	d,e	8.4
SDSS J140228.22+632133.3	0605-52353-503	N	16.91±0.01	0.2046	267±17	0.4814	2.23	10 ± 3	d,e	9.6
SDSS J140910.04+610511.5	0606-52365-315	N	17.52±0.01	0.2971	428±21[f]	0.3556	1.60	17 ± 3	c,e,g,h,j	13.9
SDSS J141622.33+513630.2	1045-52725-464	N	17.78±0.01	0.2987	240±25[f]	0.8115	1.92	26 ± 2	c,d	7.7
SDSS J144210.49−002754.1	0307-51663-065	Y	18.34±0.01	0.3717	349±28[f]	0.4404	0.99	40 ± 3	c,d,e	15.8
SDSS J152123.87+580550.6	0615-52347-311	Y[g]	17.25±0.01	0.2042	174±16	0.4857	0.96	30 ± 4	c,e	12.1
SDSS J154049.17−003342.5	0315-51663-143	Y	17.63±0.01	0.2992	300±35[f]	0.4317	1.46	19 ± 3	b,c,e	9.9
SDSS J154731.22+571959.8	0617-52072-561	Y	16.82±0.01	0.1883	254±12	0.3956	1.85	27 ± 4	c,e,g,h	8.5
SDSS J155030.75+521705.0	0618-52049-123	Y	18.38±0.02	0.4564	345±52[f]	0.5388	0.92	8 ± 2	c,e	6.8
SDSS J162746.44−005357.5	0364-52000-084	Y	17.50±0.01	0.2076	290±14	0.5241	2.76	29 ± 3	c,e	12.5
SDSS J163028.16+452036.2	0626-52057-518	Y	17.27±0.01	0.2479	276±16	0.7933	2.81	21 ± 3	d,e	10.1
SDSS J170216.76+332044.7	0973-52426-464	N	16.85±0.01	0.1785	256±14	0.4357	2.12	23 ± 5	d,e	9.2
SDSS J170955.44+582348.0	0353-51703-121	Y	17.39±0.01	0.2437	78±20[f]	0.3776	0.12	9 ± 2	c,e,g	8.5
SDSS J204249.75−062631.8	0635-52145-290	Y	18.04±0.01	0.2677	264±28[f]	0.6672	2.23	10 ± 3	c,d	6.0
SDSS J205222.58+000111.1[e]	0982-52466-602	N	17.53±0.01	0.2107	320±17	0.4635	3.04	10 ± 2	c,d	6.5
SDSS J213426.45+104313.1	0731-52460-165	N	16.89±0.01	0.2290	224±14	0.3964	1.14	14 ± 3	c,d,e,g	15.3
SDSS J213720.87−080809.5[e]	0641-52199-021	Y	17.87±0.01	0.3090	201±21[f]	0.6306	1.08	11 ± 2	d,e	7.9
SDSS J214747.04−003227.6[e]	0371-52078-307	N	18.66±0.02	0.4892	379±36[f]	0.6029	1.35	12 ± 2	a,c,e	8.3
SDSS J225125.87−092635.8[e]	0724-52254-277	N	18.33±0.02	0.4719	414±47[f]	0.6238	2.09	14 ± 2	c,e	9.7
SDSS J230053.14+002237.9[e]	0677-52606-520	N	17.59±0.01	0.2285	279±17	0.4635	2.13	19 ± 3	c,e	9.5
SDSS J230321.72+142217.9[e]	0743-52262-304	N	16.69±0.01	0.1553	255±16	0.5170	2.51	13 ± 3	c,e	8.1
SDSS J234339.73+002527.7[e]	0385-51877-596	Y	16.54±0.01	0.1858	229±14	0.2718	0.91	53 ± 4	d,e,g,h,i,j	16.6
SDSS J234728.08−000521.2[e]	0684-52523-311	N	18.42±0.02	0.4169	404±59[f]	0.7146	3.47	30 ± 3	c,e	12.7

[a] Names give truncated J2000 RA and Dec in the format HHMMSS.ss±DDMMSS.s.

[b] $\Delta\theta$ column gives an estimated angular lensing scale for each system, calculated as described in the text.

[c] [O II] $\lambda\lambda$3728 line flux in units of 10^{-17} ergs cm^{-2} s^{-1}.

[d] Other lines detected at 2.5-σ or greater. Letters specify lines as follows: a = Hδ λ4103, b = Hγ λ4342, c = Hβ λ4863, d = [O III] λ4960, e = [O III] λ5008, f = [N II] λ6550, g = Hα λ6565, h = [N II] λ6585, i = [S II] λ6718, j = [S II] λ6733.

[e] See § 4.2 for remarks on follow-up imaging of these systems.

[f] Velocity dispersion (σ_v) value possibly unreliable: either too high ($>$ 420 km s^{-1}), too low to be properly resolved ($<$ 100 km s^{-1}), or LRG spectrum median signal-to-noise per pixel too low ($<$ 10).

[g] SDSS-DR1 contains lower signal-to-noise spectra of these systems from earlier observations, with Plate-MJD-Fiber values of 414-51901-266 (for SDSS J0324) and 612-52079-607 (for SDSS J1521).

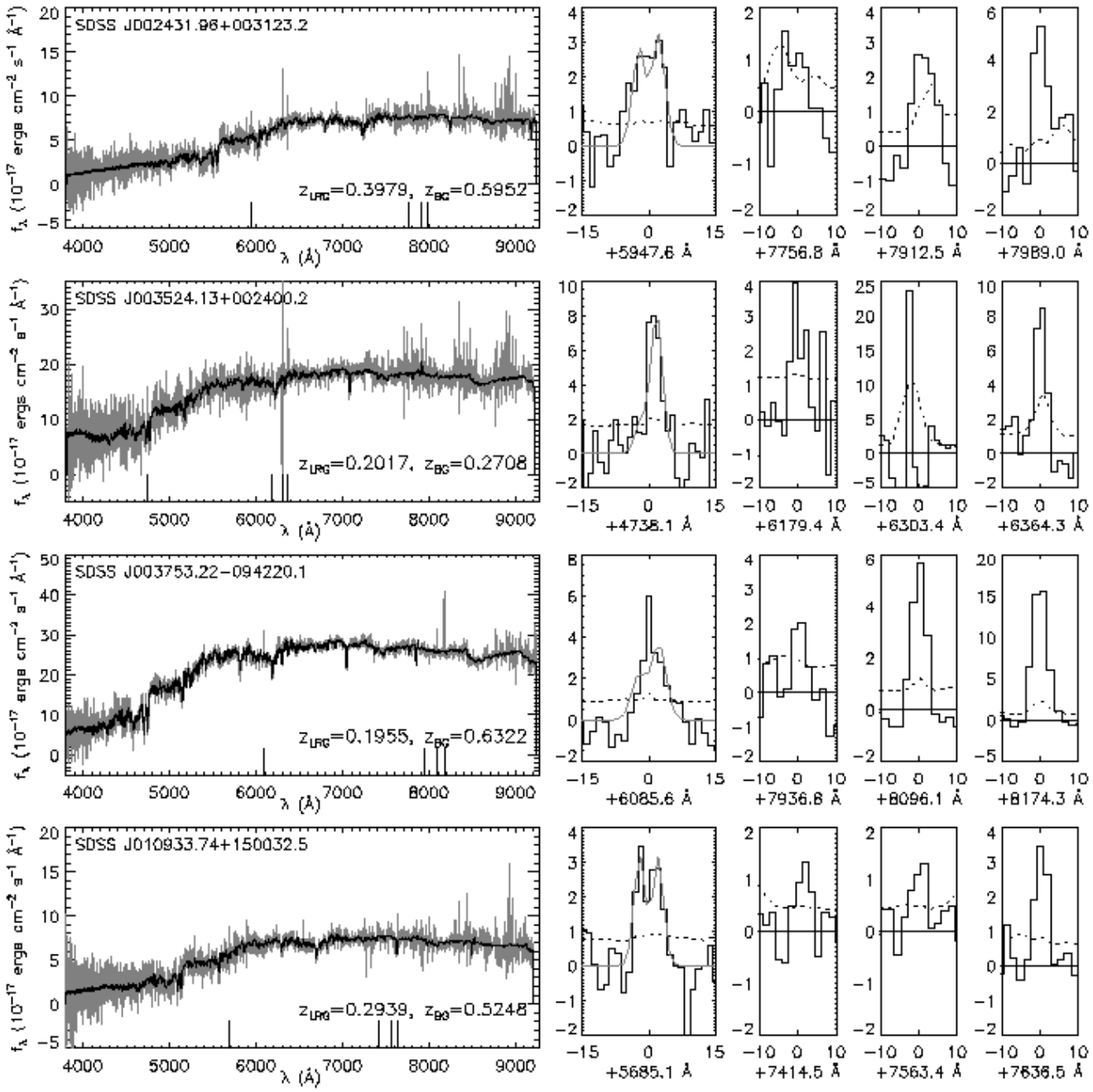

FIG. 2.— SDSS LRG spectra with confirmed background-galaxy emission features. In the full-spectrum plots, gray lines show data, black lines show best-fit model spectrum, and long ticks along bottom margin indicate the position of redshifted [O II] $\lambda\lambda$3728, Hβ λ4863, [O III] λ4960, and [O III] λ5008 background emission. Smaller windows show zooms of the residual (data − model) spectra at the positions of these same redshifted emission lines. Dashed lines in the smaller windows show the 1-σ noise level, rescaled as described in Appendix A. Gray lines in the [O II] $\lambda\lambda$3728 zoom show the double-Gaussian fit; the zero-flux line is drawn in the other three zooms. The spectroscopic resolution is $\lambda/\Delta\lambda \approx 1800$. Note the changing vertical scales.

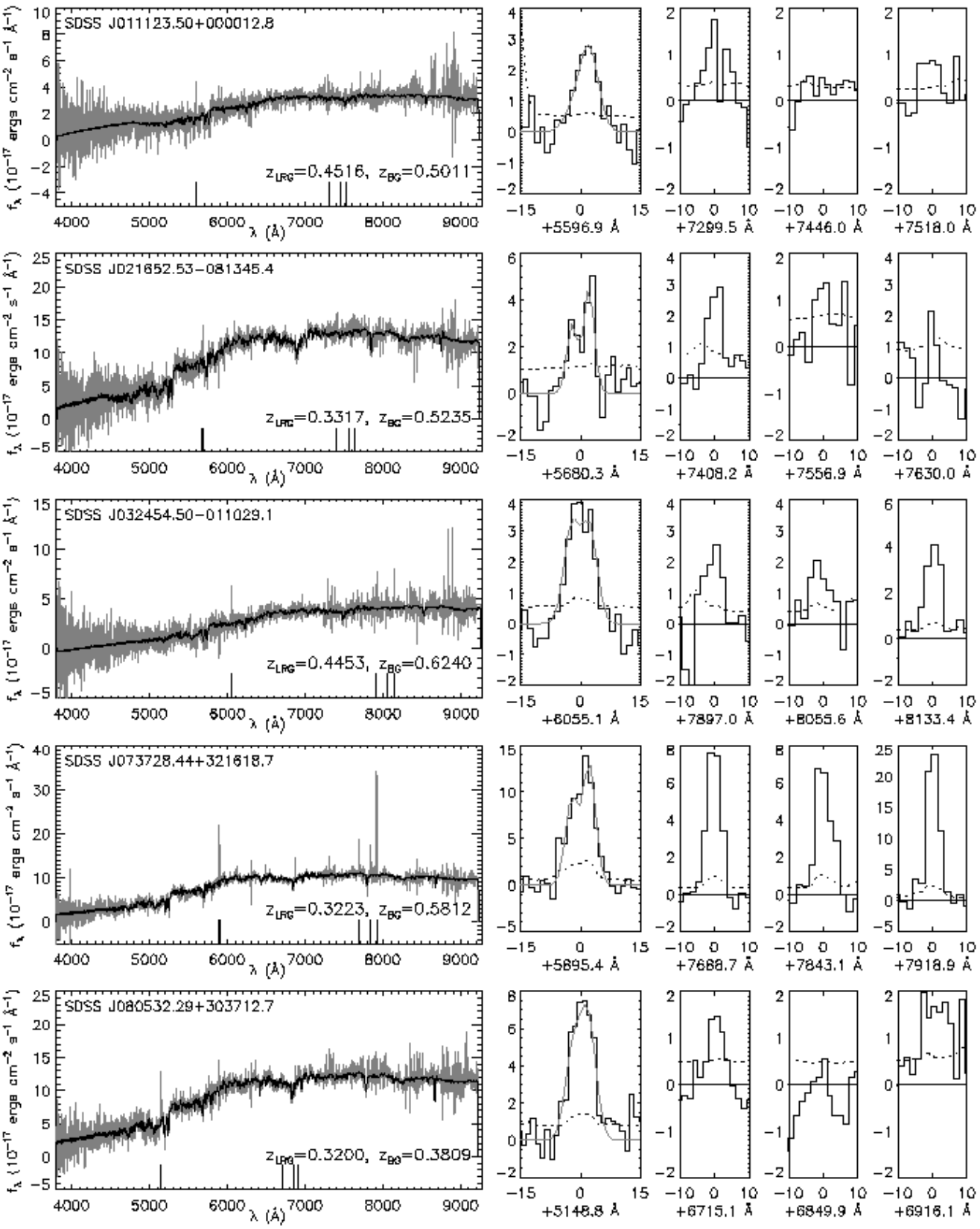

FIG. 2.— Continued

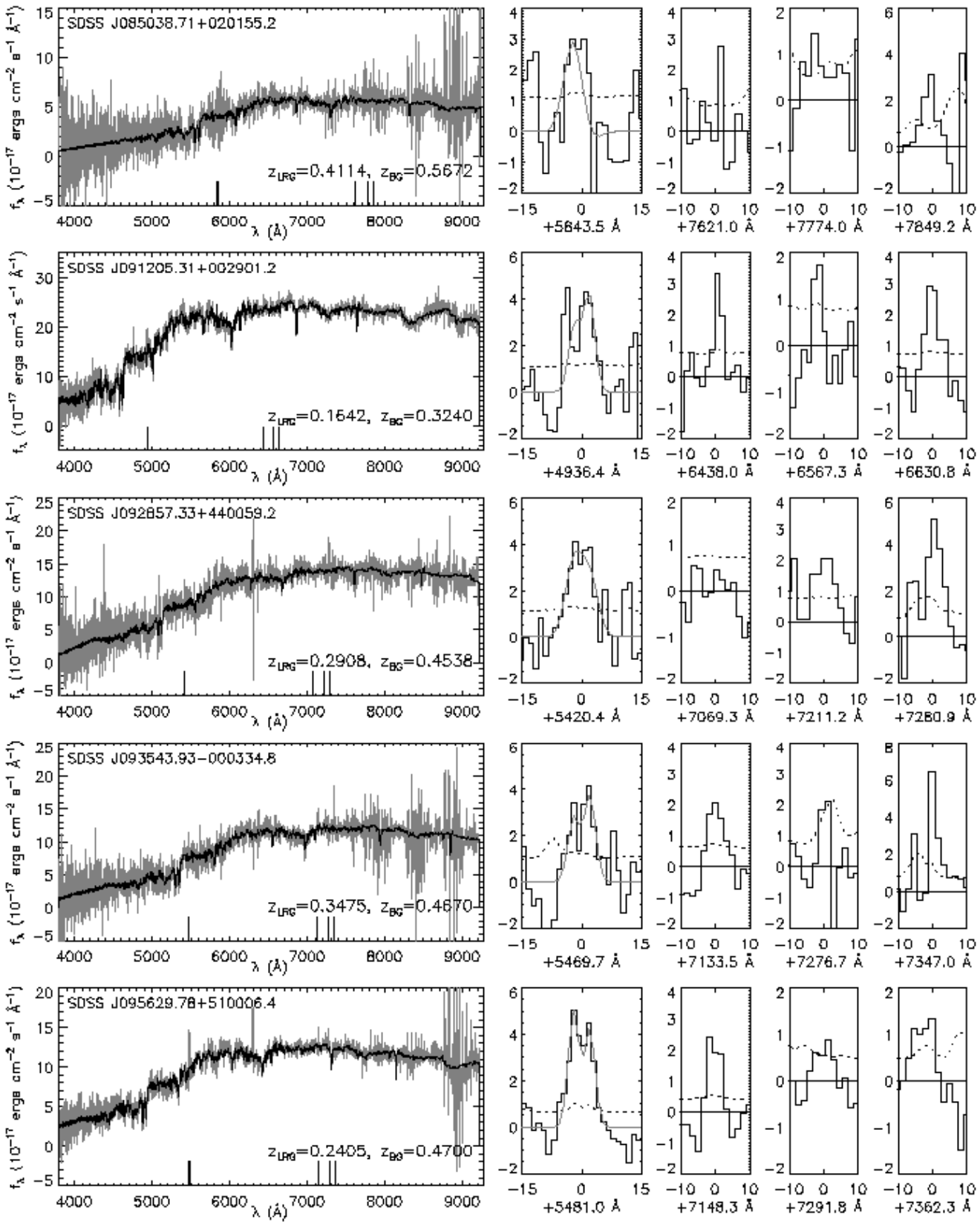

FIG. 2.— Continued

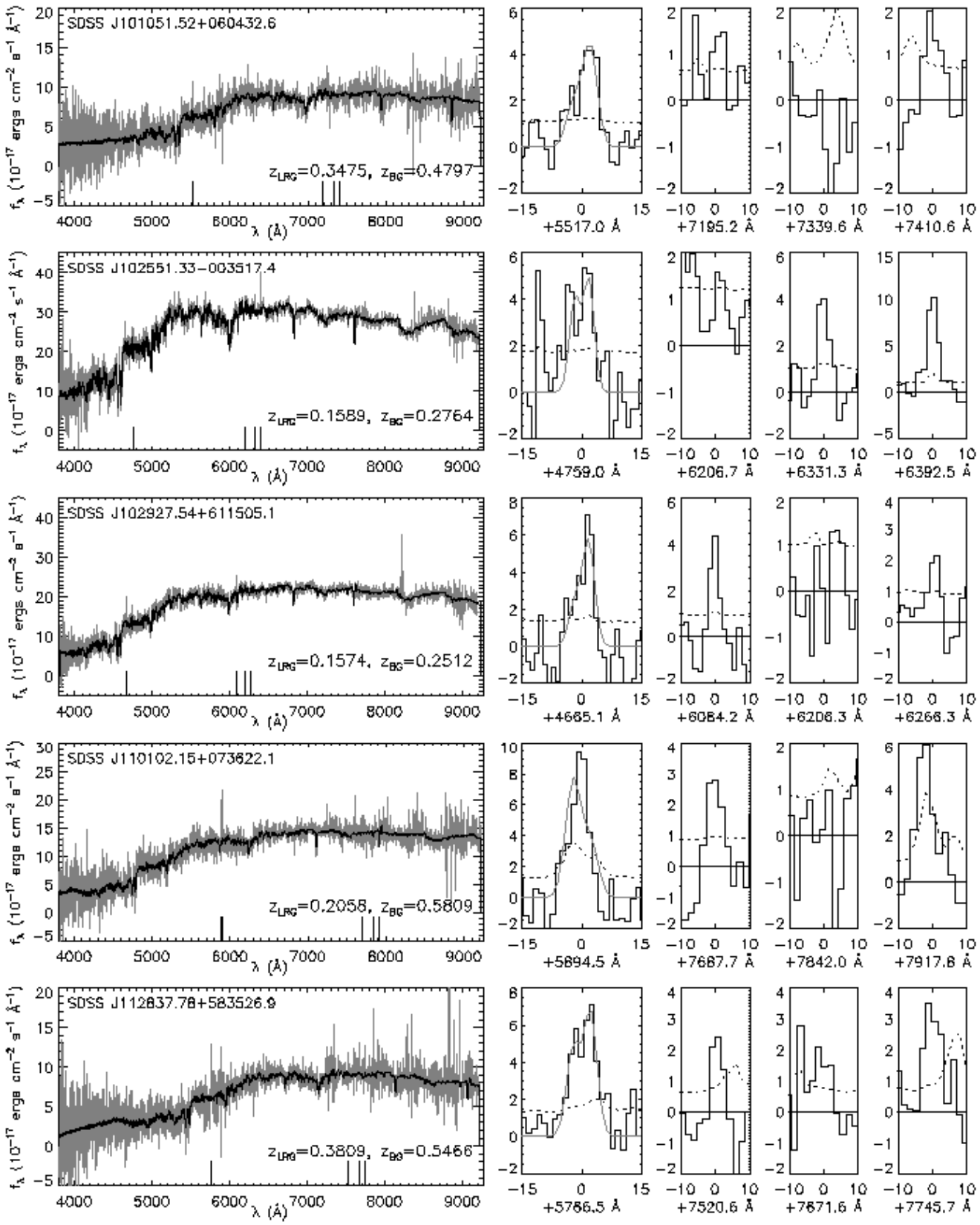

FIG. 2.— Continued

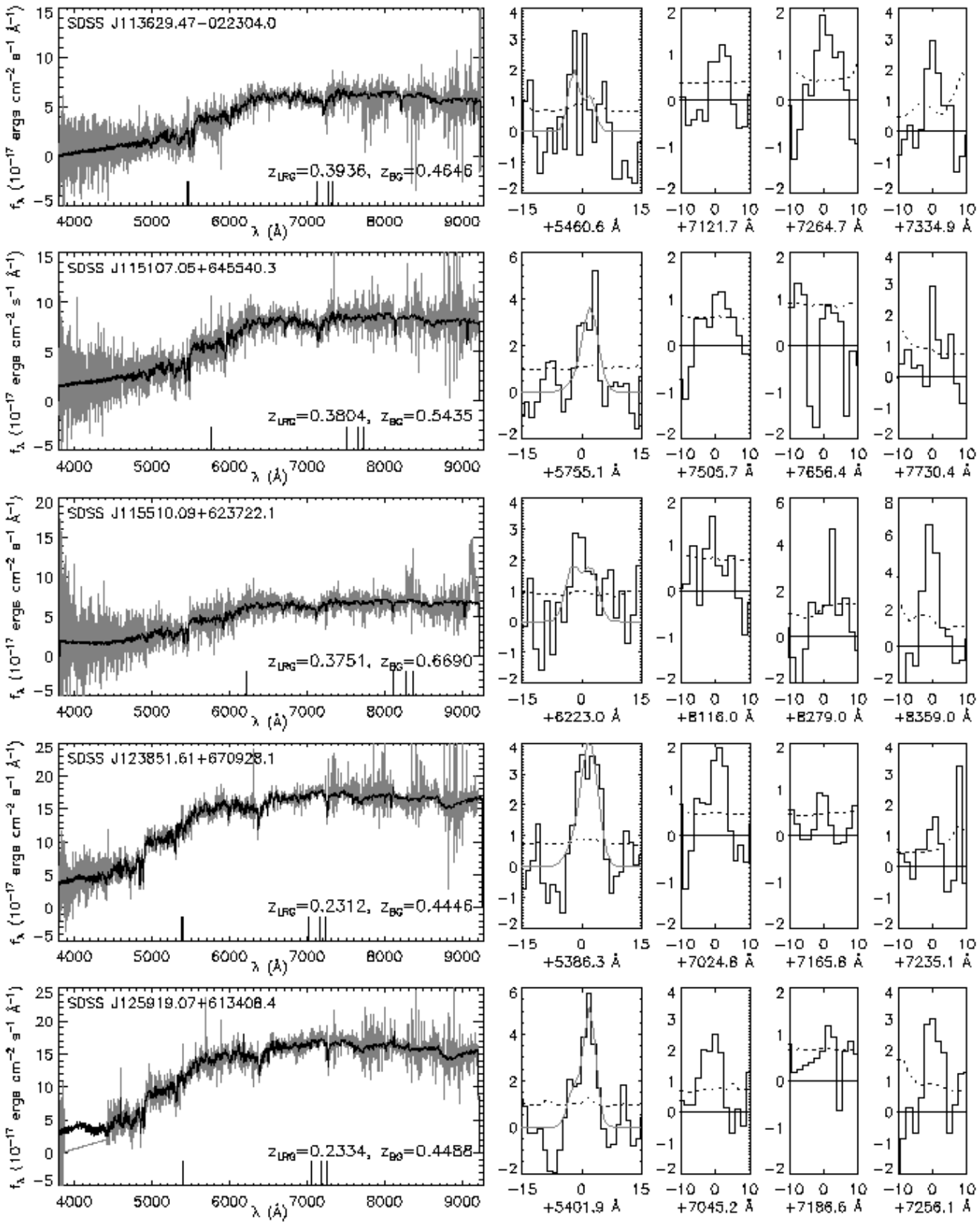

FIG. 2.— Continued

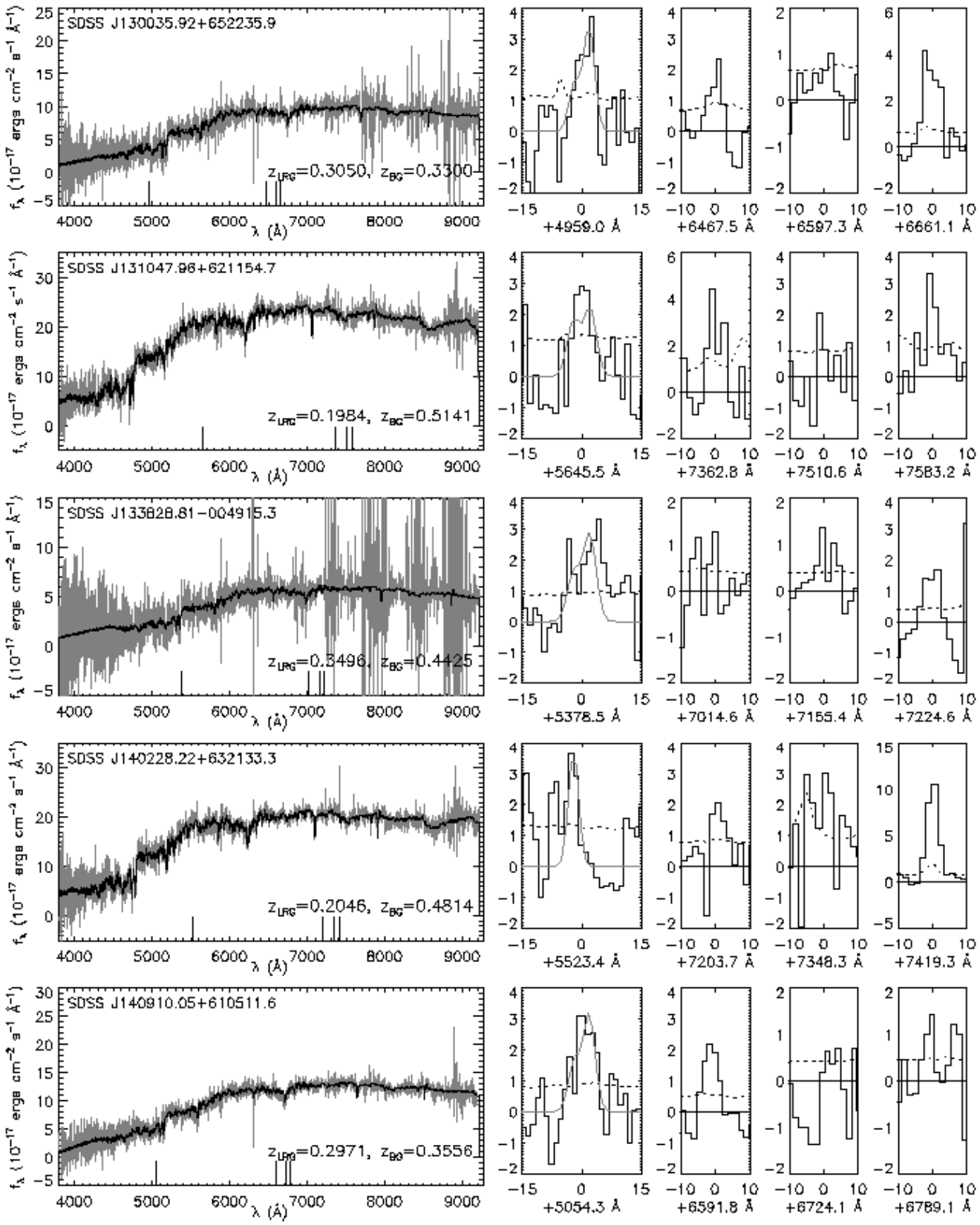

FIG. 2.— Continued

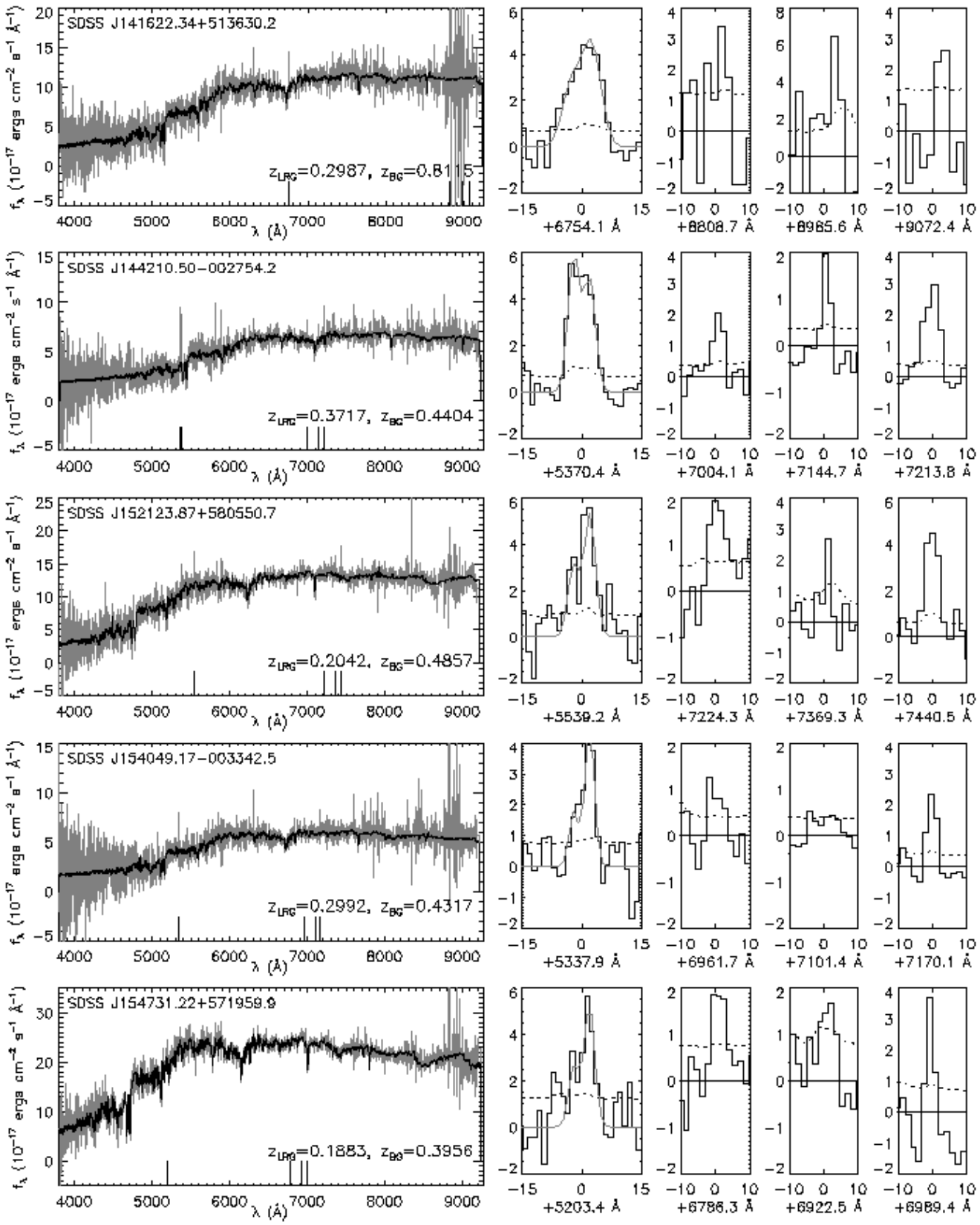

FIG. 2.— Continued

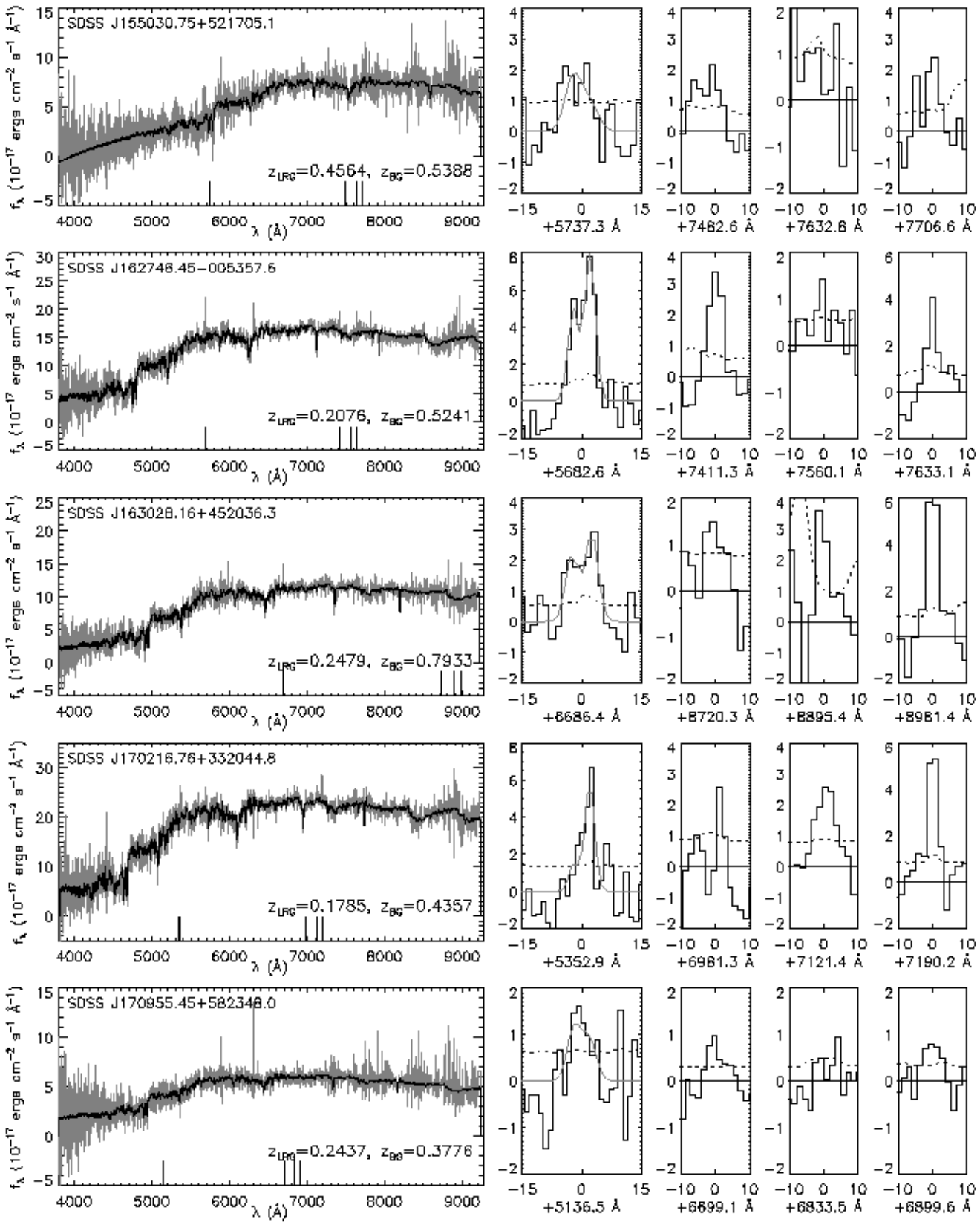

FIG. 2.— Continued

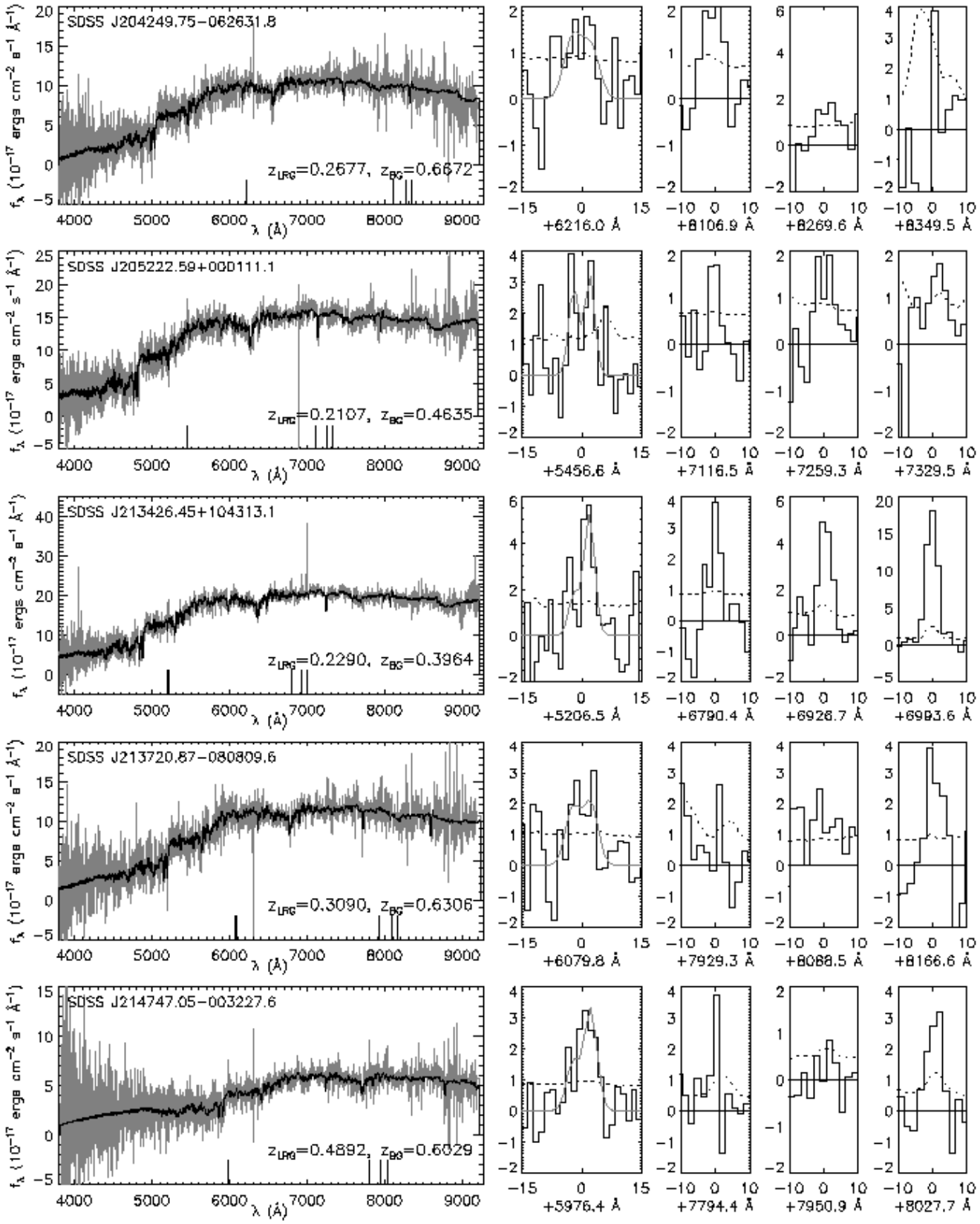

FIG. 2.— Continued

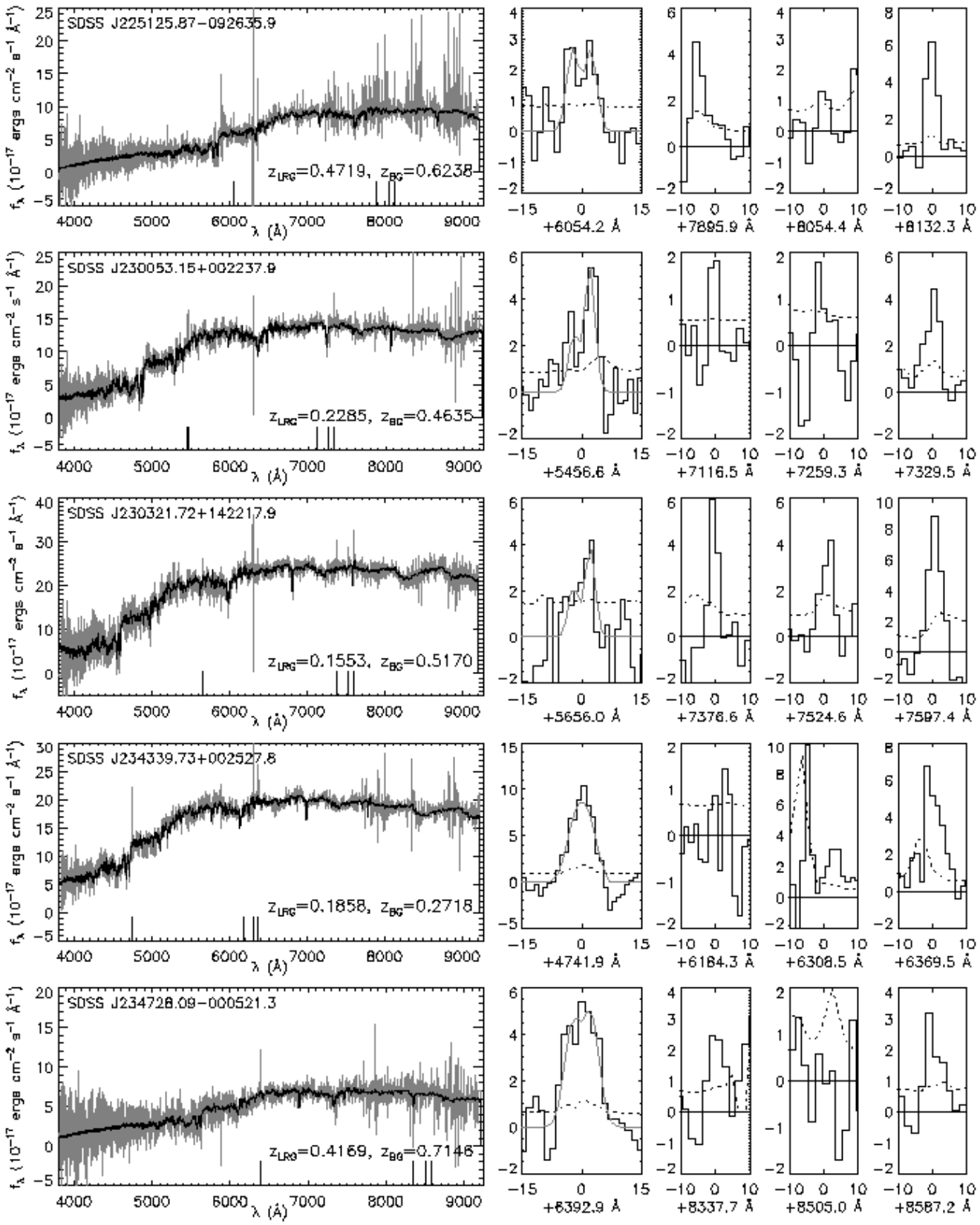

FIG. 2.— Continued

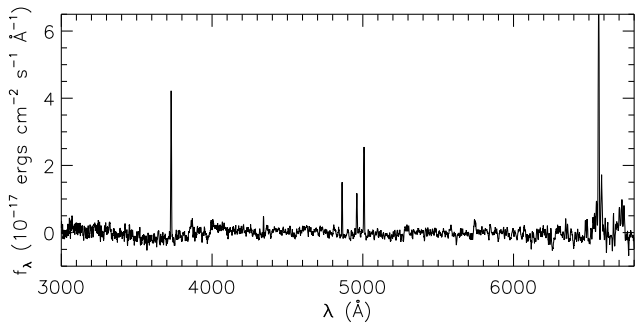

FIG. 3.— Median rest-frame spectrum of background galaxies detected in our residual LRG spectra, created as described in the text and smoothed with a 5-pixel boxcar. Note the continuum break at 4000Å and the absorption feature at 5270Å, which are not discernible in the individual residual spectra. Also evident are the emission lines Hγ λ4342, Hα λ6565, [N II] λ6550, [N II] λ6585, [S II] λ6718, and [S II] λ6733, in addition to the emission lines for which we select.

band exposures (120s each) were taken on the nights of 2003 August 1 and 2 with the Magellan Instant Camera (MagIC) CCD imager and active telescope optics (Schechter et al. 2003). Conditions were similar on both nights: non-photometric due to cirrus clouds, and with $\sim 0\farcs8$ median FWHM seeing. For the majority of these systems, the images present no significant evidence for or against the presence of strong lensing; we describe the exceptions here. One system, SDSSJ0035, is almost certainly not a strong lens: a relatively g-bright galaxy can be seen clearly in the images, approximately $2\farcs6$ offset from the LRG. This far exceeds the anticipated lensing scale of about $0\farcs4$ reported in Table 1. The images of SDSSJ2147 reveal a bluer galaxy approximately $1\farcs3$ to the South, about at the limit of the estimated lensing scale. We see no particular evidence for strong lensing, but deeper observation of this system could be of interest. Two systems, SDSSJ0037 and SDSSJ0216, show evidence of multiple imaging. Figure 5 shows g-band images of these two systems, along with difference images created by smoothing aligned i-band images with a Gaussian kernel in order to suppress noise and match the slightly worse g-band seeing, then fitting this smoothed i-band LRG image to the g-band image and subtracting it. The difference images are then smoothed with a Gaussian kernel of FWHM $\approx 0\farcs4$ in order to bring out coherent features; they show strong evidence of multiply imaged, relatively blue sources. SDSSJ0037 seems likely to be a double-image lens. It is tempting to identify quadruple-image morphology in the SDSSJ0216 difference image, but the level of noise recommends caution. Narrow-band imaging or integral-field spectroscopy should permit quantitative study of these systems and of those for which broadband imaging is inconclusive. *HST* imaging of any confirmed lenses using the narrow-band ramp filter set of the *Advanced Camera for Surveys* could also be pursued to obtain a highly resolved picture of lensed line-emitting regions and permit even more detailed study of the lensing mass distributions.

The degree of lensing that will be present in a particular system will depend on the impact parameter (angular offset) of the background galaxy in the source plane relative to the center of the LRG: the smaller the impact parameter, the more lensing will be seen. To obtain a rough estimate of the number of lenses within our sample, we can guess at the unlensed surface brightness distribution of our background galaxies, compute lensed images under an assumed lens model, smear to account for seeing, and integrate over the $3''$-diameter SDSS spectroscopic fiber, then compare to the [O II] line flux values that we have observed. To interpret the results in terms of lensing probabilities we must also invoke an [O II] $\lambda\lambda$3728 luminosity function (LF). Appendix B describes the details of a lensing probability calculation of this nature that we have carried out. The results suggest that a total of 19 out of 49 systems are likely to be strong lenses—that is, we expect approximately 19 systems to have source-galaxy impact parameters less than the critical value for multiple imaging. It is important to recognize, though, that the "lenses-or-not" question does not have as straightforward an answer for extended sources as it does for point sources. Different regions of our background galaxies will be lensed by different amounts, and in general some but not all of the galaxy can be multiply imaged. It is more appropriate to ask *how much* lensing is present in any given system.

There is a sense in which the unknown degree of lensing in our systems may prove to be of scientific interest. Binney (2003) raises the concern that current strong-lensing evidence for massive dark-matter halos in elliptical galaxies may reflect a selection bias. We quote directly: "even if only a minority of ellipticals have massive dark halos, nearly all the observed lenses will belong to that minority." Our LRG sample, in contrast, has not been selected for lensing, but rather for back-lighting. The true incidence of lensing within our sample will thus constitute a test of whether or not the dark halos in currently known lenses are in fact generic to early-type galaxies.

We present a comparison between our lens candidate LRGs and the full 51,000 LRG spectroscopic sample in Figure 6. The lens candidate LRGs seem somewhat skewed towards brighter magnitudes. The conservative interpretation is that the broadband selection properties of fainter LRGs are more easily perturbed by background galaxies, but it may also reflect a lensing signal, with more massive galaxies providing more magnification. If the logarithmic slope of the underlying [O II] LF is steeper than -1 at the luminosities probed by our survey, then magnified lines of sight should show a statistically enhanced number of [O II] emitters (Turner, Ostriker, & Gott 1984). Hogg et al. (1998) find the logarithmic [O II] LF slope to be steeper than -1 for line luminosities $\gtrsim 10^{42}$ ergs s^{-1}, whereas the median observed [O II] luminosity in our sample is of order 10^{41} ergs s^{-1} (again, we have taken $H_0 = 70$ km s^{-1} Mpc^{-1}). These numbers suggest that magnification bias is not the explanation for the observed brightness of our lens candidates relative to the full LRG sample, but a more definite statement must await follow-up observations that capture the total background line flux.

Most known gravitational lens systems have been selected on the basis of some combination of source properties and lens cross section, whereas the SDSS LRG sample is selected based on colors and magnitude. It is therefore of interest to compare known early-type lens

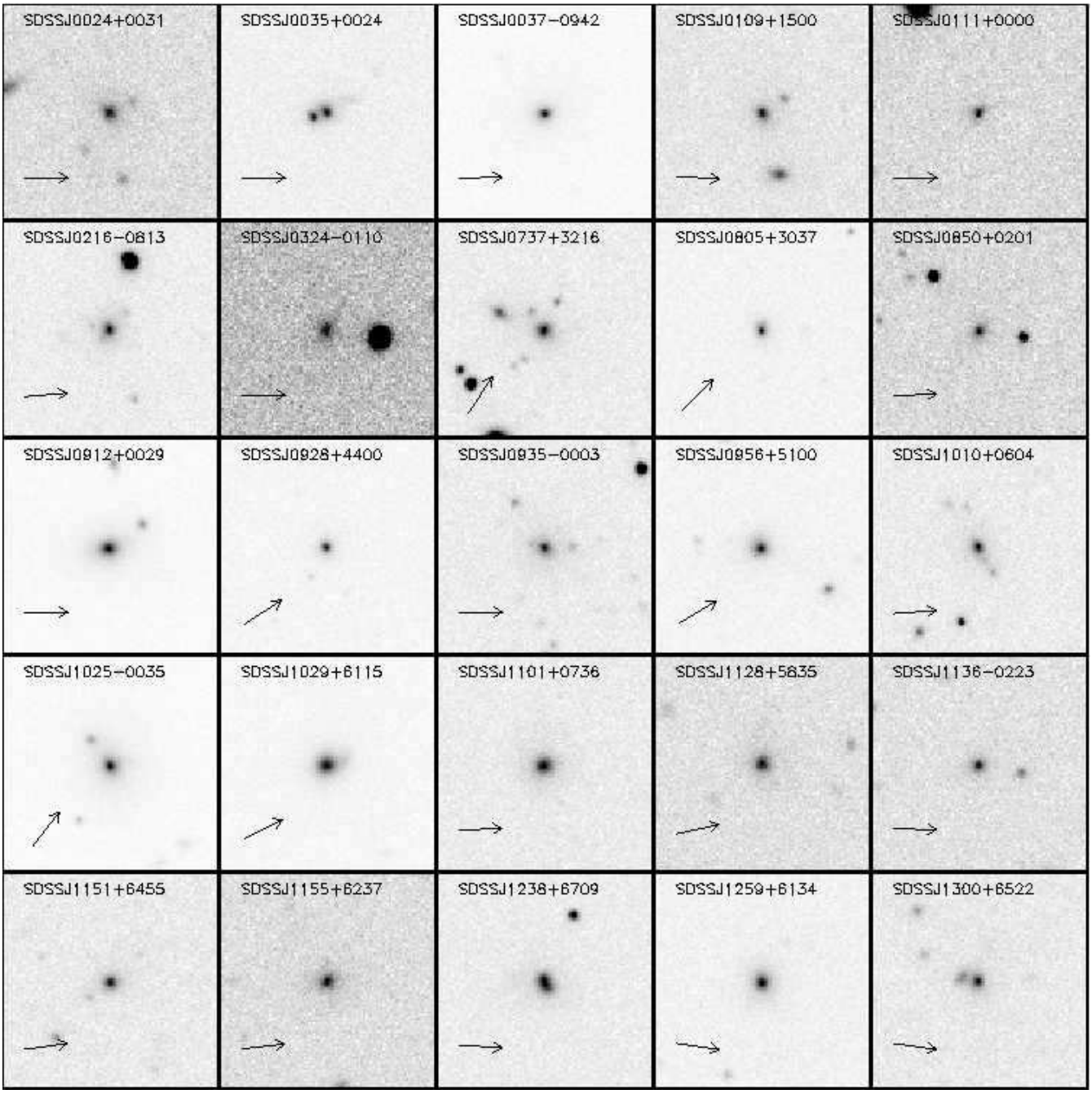

FIG. 4.— $40'' \times 40''$ SDSS r postage-stamp images of LRG systems with confirmed background emission. Gray-scaling is linear from -3σ sky noise (white) to LRG peak brightness (black). Arrows point North; East is 90° counterclockwise from North (i.e., as seen on the sky).

galaxies to our candidate lenses, although this is difficult since we do not currently have truly comparable observations of the two samples. Figure 7 presents our best attempt at such a comparison for lens velocity dispersions and apparent magnitudes as a function of redshift[10], with *HST* known-lens data taken from Rusin et al. (2003a). The known-lens velocity dispersions are estimated from lensed image separations in the manner described by Kochanek et al. (2000); they may be systematic overestimates if these lenses are superimposed on the "mass sheet" of a high-density environment (Holder & Schechter 2003). Magnitude comparison is made by transforming SDSS g- and r-band magnitudes to Johnson-Morgan V-band using the observed transformation of Smith et al. (2002). We see that our LRG lens candidates are in general of greater velocity dispersion than known lenses, and in the redshift range where the two samples overlap, the LRGs are more luminous. The brightness of the LRGs combined with the relative faintness of the background galaxies in our sample suggests that any confirmed LRG lenses would be well suited to the type of detailed lens stellar-dynamical studies described by Treu & Koopmans (2002) and

[10] We plot these quantities as a function of redshift to avoid the issue of evolutionary and k corrections.

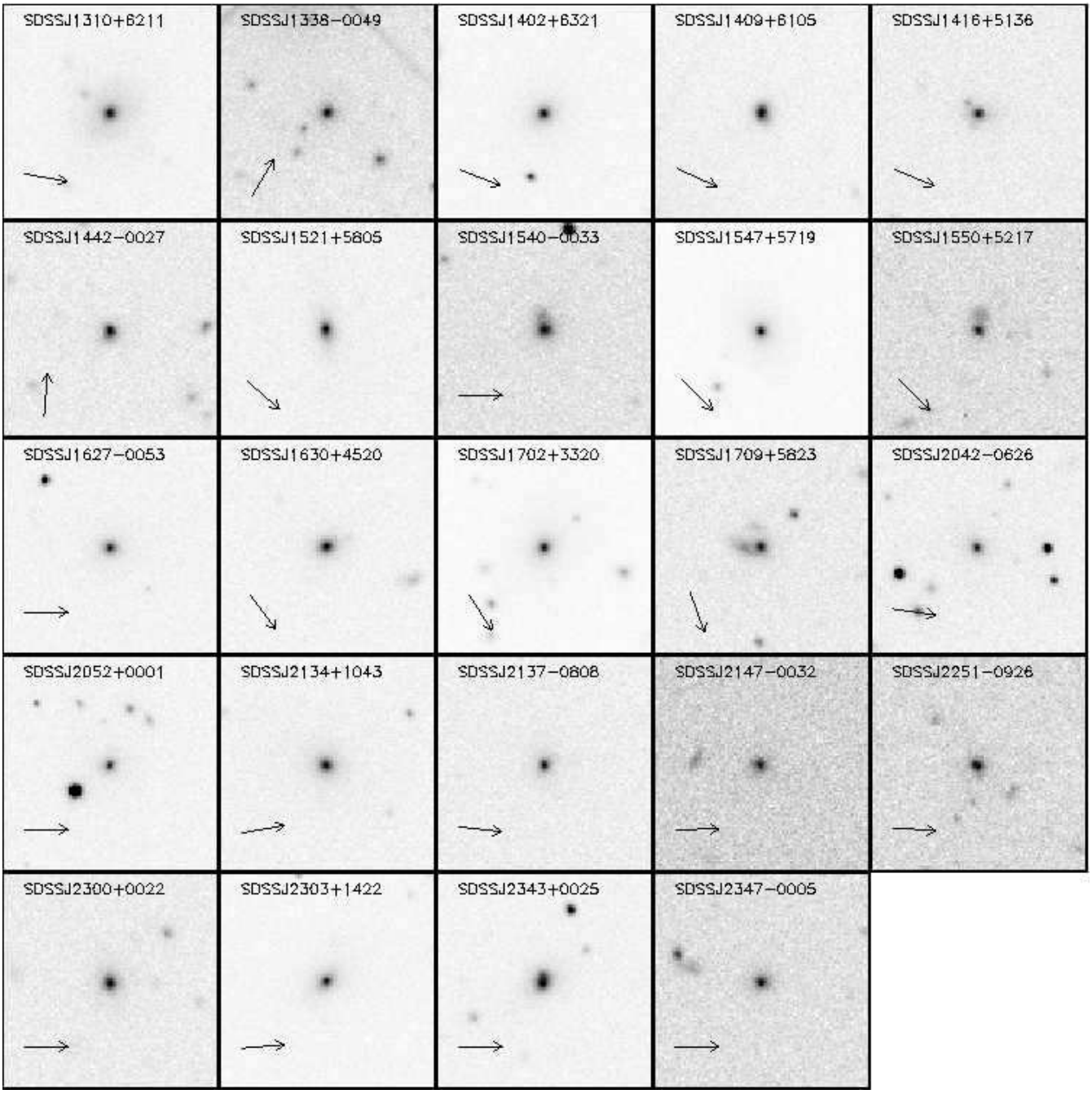

FIG. 4.— Continued

Koopmans & Treu (2003).

5. CONCLUSIONS

We have presented a catalog of candidate strong galaxy-galaxy gravitational lens systems detected spectroscopically within the Sloan Digital Sky Survey. These systems have known foreground *and* background redshifts; only the detailed spatial alignment of foreground and background galaxies remains unknown. We plan to conduct integral-field spectrographic follow-up observations of these systems, which will allow us to resolve the spatial distribution of the background nebular line emission that we have detected. These observations should confirm a substantial number of lenses within our candidate sample, with many lensed galaxies at lower redshift than any other currently known lensed extra-galactic optical sources. Any lenses confirmed within our sample will be of considerable interest for the study of early-type galaxy mass distributions, and could have implications for lens-time-delay H_0 measurements and anomalous quasar-lens flux ratios. Our sample demonstrates the feasibility of the emission-line-based spectroscopic lens search technique within the SDSS and other redshift surveys, and we plan to extend the search to higher source redshifts in the near future. We have also developed and applied a method for abating the influence

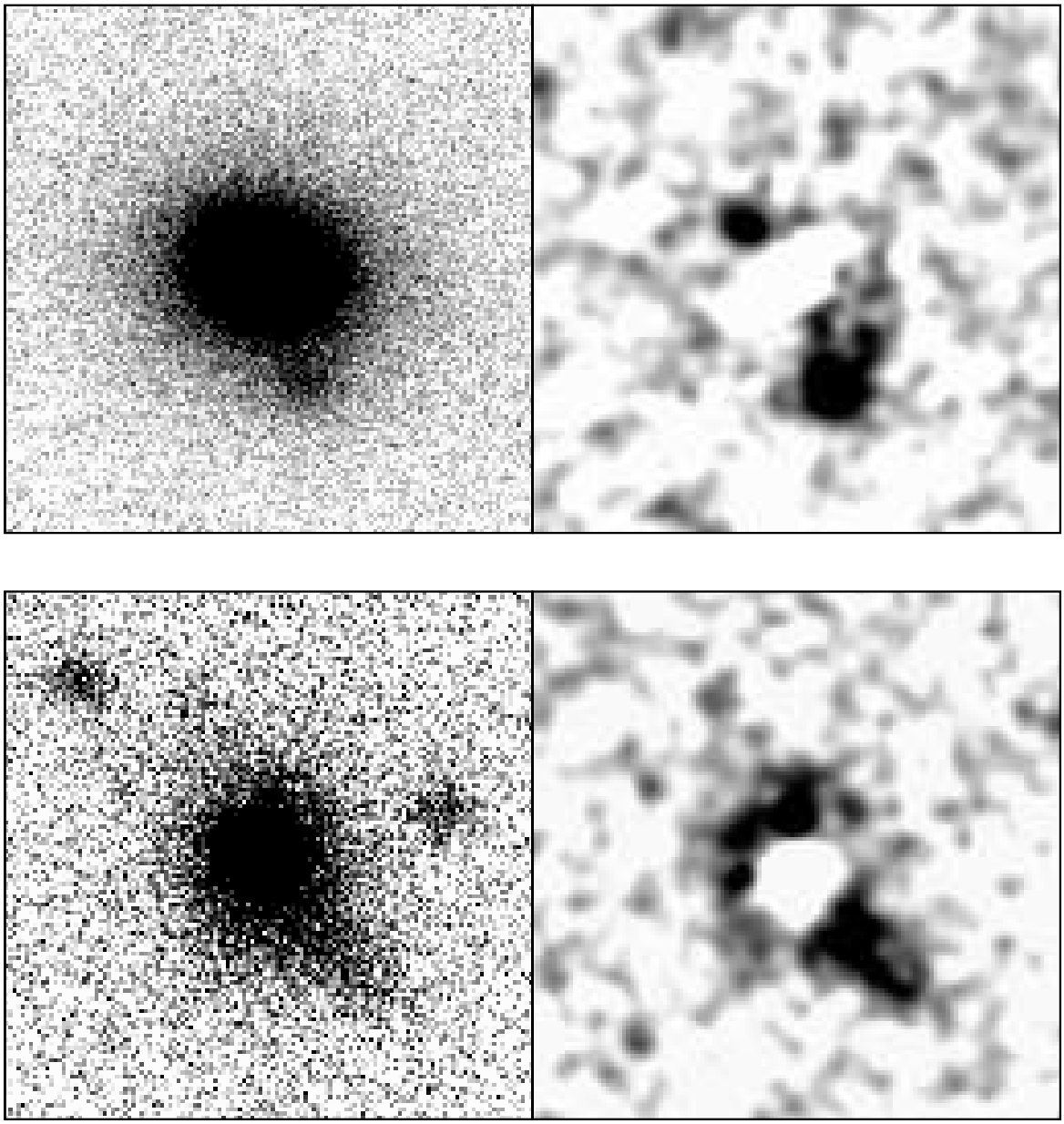

FIG. 5.— MagIC $8\farcs8 \times 8\farcs8$ images and difference images of lens candidates SDSSJ0037 (top) and SDSSJ0216 (bottom). Left-hand panels show 120-s g-band images of the two systems; right-hand panels show smoothed $g-i$ difference images created as described in the text. Note the evidence for multiply imaged, relatively blue objects in the difference images. (In these images, North is left and East is up—reversed parity from what is seen on the sky.)

of night sky emission-line residuals in the 7000–9000-Å range that allows us to detect [O III] and Hβ emission over the redshift range $z \sim 0.4$–0.8 without an excess of false-positive detections.

Funding for the creation and distribution of the SDSS Archive has been provided by the Alfred P. Sloan Foundation, the Participating Institutions, the National Aeronautics and Space Administration, the National Science Foundation, the U.S. Department of Energy, the Japanese Monbukagakusho, and the Max Planck Society. The SDSS Web site is http://www.sdss.org/.

The SDSS is managed by the Astrophysical Research Consortium (ARC) for the Participating Institutions. The Participating Institutions are The University of Chicago, Fermilab, the Institute for Advanced Study, the Japan Participation Group, The Johns Hopkins University, Los Alamos National Laboratory, the Max-Planck-Institute for Astronomy (MPIA), the Max-Planck-Institute for Astrophysics (MPA), New Mexico State University, University of Pittsburgh, Princeton University, the United States Naval Observatory, and the University of Washington.

The authors thank Paul Hewett for his constructive referee report. ASB thanks Paul Schechter and Hsiao-Wen Chen for valuable discussion and consultation.

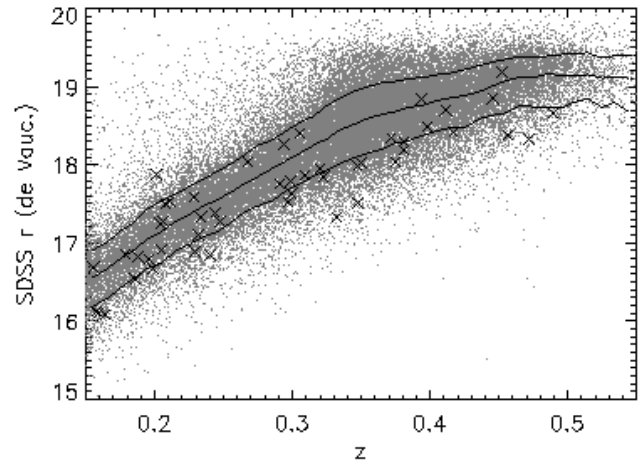

FIG. 6.— Comparison of lens-candidate LRGs (crosses) to full LRG sample (gray dots) in the magnitude-redshift plane. The three black lines show the redshift-dependent median de Vaucouleurs r magnitude of the full sample and the 84th- and 16th-percentile r values.

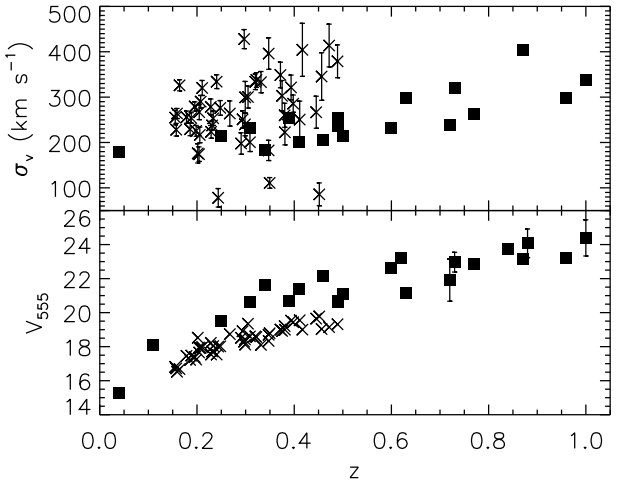

FIG. 7.— Comparison of candidate LRG lens galaxies (crosses) with known early-type lenses with known lens redshifts (filled squares). *Top panel*: comparison of velocity dispersions σ_v measured for LRG lens candidate galaxies and inferred from image separations $\Delta\theta$ in known early-type lens systems with known lens and source redshifts. Image separations are taken from Rusin et al. (2003a), and conversion to velocity dispersion estimates is made via Equation 5 of Kochanek et al. (2000). For visual clarity, we omit error bars on the latter data points; Kochanek et al. (2000) estimate 10% errors in the $\Delta\theta \rightarrow \sigma_v$ conversion. *Bottom panel*: V-band magnitude comparison. SDSS g- and r-band magnitudes are converted to Johnson-Morgan V via the observed transformation of Smith et al. (2002); we have also corrected for an 0.2-magnitude systematic error in the SDSS magnitudes (Abazajian et al. 2003). Error bars on SDSS photometric quantities are smaller than plotted symbol sizes. Known-lens photometric data taken from Rusin et al. (2003a). All magnitudes have been corrected for galactic extinction using Schlegel, Finkbeiner, & Davis (1998) dust maps.

APPENDIX

A. NOISE MODELING

If the model of a purely Gaussian noise spectrum described by σ_λ were correct, then the distribution of scaled residual specific fluxes

$$x_\lambda \equiv f_\lambda^{(r)}/\sigma_\lambda \tag{A1}$$

across all spectra would be Gaussian with unit variance for all wavelengths λ. This is unfortunately not the case in our sample. Imperfect night-sky emission-line subtraction and other miscellaneous effects give rise to an excess of "high-significance" outliers beyond the predictions of a Gaussian model, leading to a deluge of false-positive astronomical emission-line candidates when the procedure described in § 3.1 is applied, particularly in the 7000–9000-Å region of the spectrum where the [O III] λ5008 line at redshifts $z \approx 0.4$–0.8 appears. The most drastic solution is simply to mask all sky-afflicted wavelengths. Rather than concede such vast spectral coverage (which would drastically reduce our survey volume), we describe the observed distribution of scaled residual specific fluxes x_λ within the LRG sample with a more detailed empirical noise model. The generally Gaussian behavior of scaled residuals at low significance combined with the excess of high-significance residuals is well described by a mixture of Gaussian and Laplace distributions, expressed parametrically as

$$p(x)\,dx = \left[a\exp(-x^2/2\sigma_g^2) + b\exp(-|x|/\sigma_e)\right]\,dx \tag{A2}$$

(For history and applications of the Laplace distribution, see Kotz, Kozubowski, & Podgórski 2001) The parameters of this distribution are wavelength-dependent, but we suppress this dependence in out notation. The values of a and b are related by normalization:

$$\int_{-\infty}^{+\infty} p(x)\,dx = \sqrt{2\pi}\sigma_g a + 2\sigma_e b = 1 \quad . \tag{A3}$$

We also fix the following relations between parameters, based on strong correlations observed in free-parameter fits to the distribution at each wavelength:

$$\sigma_e = \sigma_g - 0.38 \quad , \tag{A4}$$

$$b = 0.09 \times \sigma_g(a+b) \quad . \tag{A5}$$

The result is a one-parameter noise model to fit to the distribution of x_λ across the sample at each wavelength. (The numerical values 0.38 and 0.09 are fixed by minimizing the sum of binned χ^2 values for fits across all wavelengths.) We relax conditions (A4) and (A5) and fit freely for σ_e and b at a few isolated locations in the spectrum, where the effects of sky-subtraction residuals are especially strong and the correlations that suggest (A4) and (A5) break down—regions near 5577 Å, 5894 Å, 6305 Å, and 6366 Å. Additionally, some regions of some spectra are characterized by extreme and correlated excess variance, so for each spectrum we convolve $|x_\lambda|$ capped at 5 (to limit the influence of single pixels) with a 100-pixel boxcar filter and exclude from the noise-modeling sample any pixels within a boxcar whose value exceeds 1.25.

We use our fitted noise model to re-scale the reported σ_λ values such that the new distribution $p(x)\,dx$ of scaled residual flux values at each wavelength becomes Gaussian, while preserving the position of individual x-values within the cumulative distribution, then proceed as described in § 3.1. Both the reported noise σ_λ *and* the measured residual flux values $f_\lambda^{(r)}$ contain information about the actual error in the presence of imperfect subtraction, so it is sensible to base an effective noise rescaling on their ratio x_λ in this manner. By fitting the noise distribution parameters independently at each wavelength, we also capture the localized effects of individual night-sky lines.

B. LENSING PROBABILITIES

Our strategy for assessing lensing probabilities in our sample centers on the construction of an approximated probability density $p(b)\,db$ for the unknown impact parameter b of the background galaxy in each system. The following observed quantities are input to the calculation: the LRG and background redshifts, the LRG velocity dispersion, the background [O II] $\lambda\lambda$3728 line flux received by the 3″-diameter spectroscopic fiber, and the median seeing for the spectroscopic plate under consideration. We also make use of the [O II] line luminosity function (LF) reported by Hogg et al. (1998). We adopt the same SIS model for the LRG mass distribution as was used to obtain the $\Delta\theta$ values in Table 1, and we model the background galaxies as exponential disks with a half-light radius of approximately 3 kpc (fixed to 0.″5 at $z = 0.5$).

For each system, we explore a range of impact parameters b from 0 to 5″. At each b-value, we generate a lensed image of the model background galaxy, then convolve it with a Gaussian point-spread function corresponding to the median seeing reported in the spectroscopic plate header. We then integrate the image over a 3″-diameter circular fiber aperture centered on the model lens. The result is a tabulated function $f(b)$ giving the fraction of the intrinsic flux received by the fiber; that is, if the total galaxy line flux were S in the absence of lensing and limited fiber sampling, the [O II] line flux received by the spectroscopic fiber from a background galaxy with a source-plane offset b would be $S_{\rm fib} = f(b)S$. In general $f(b)$ may be greater or less than one due to the competing effects of lens magnification and incomplete sampling by the fiber.

Next we adopt the [O II]-emitter LF reported by Hogg et al. (1998) by fitting a Schechter function to their Figure 6. After converting from logarithmic units, the number of [O II] emitters per unit volume in an interval dL at line luminosity L is well approximated by

$$\phi(L)\,dL \propto L^{\alpha}\exp(-L/L_{\star})\,dL \quad , \tag{B1}$$

with $\alpha \simeq -1.3$ and $L_{\star} \simeq 3.4\times10^{42}$ ergs s^{-1} (the overall normalization is unimportant for our purposes). We make a crude conversion from their assumed $(\Omega_M,\Omega_\Lambda) = (0.3, 0)$ universe to our cosmology by scaling their reported luminosities up by a factor of 1.2: the ratio of squared luminosity distances in our cosmology to theirs ranges from 1.16 at $z = 0.3$ to 1.27 at $z = 1$, and the bulk of galaxies in their study fall within this range. Assuming the form of the LF does not evolve, it corresponds to an intrinsic flux function at any redshift z for the number of galaxies per unit redshift per unit solid angle within some intrinsic flux range dS about S:

$$\psi(z,S)\,dS = N(S,z)\,S^{\alpha}\exp(-S/S_{\star})\,dS \quad , \tag{B2}$$

with the same α as the LF and $S_{\star} = L_{\star}/[4\pi D_L^2(z)]$, where $D_L(z)$ is the luminosity distance to redshift z. $N(S,z)$ is a flux- and redshift-dependent normalization, the form of which will prove unimportant.

We can now derive a joint probability density function (PDF) for the observation of an [O II]-emitting galaxy behind a given LRG at impact parameter b, redshift z, and with line flux $S_{\rm fib}$ in the fiber by setting the differential probability proportional to the corresponding expected differential number count and making use of the known relationship of $S_{\rm fib}$ to intrinsic flux S through $f(b)$:

$$\begin{aligned} p(b,z,S_{\rm fib})\,db\,dz\,dS_{\rm fib} &\propto \psi(z,S)\,d\Omega\,dz\,dS \\ &= \psi[z,S_{\rm fib}/f(b)]\,(2\pi b\,db)\,dz\,[dS_{\rm fib}/f(b)] \quad . \end{aligned} \tag{B3}$$

The term $d\Omega = 2\pi b\,db$ represents the solid angle in the source plane of an annulus of radius b and thickness db. The *observed* quantities $S_{\rm obs}$ and $z_{\rm obs}$ for the system are equal to the system's true $S_{\rm fib}$- and z-values plus some observational noise that is independent of b, so assuming the noise is small relative to the scale on which the joint PDF varies, we may reinterpret the joint PDF as an approximate conditional PDF on b given $z_{\rm obs}$ and $S_{\rm obs}$:

$$p(b;z_{\rm obs},S_{\rm obs})\,db = N'(z_{\rm obs},S_{\rm obs})\,b\,[f(b)]^{-1}\,\psi[z_{\rm obs},S_{\rm obs}/f(b)]\,db \quad . \tag{B4}$$

The normalization $N'(z_{\rm obs},S_{\rm obs})$ need not be derived explicitly, since we can simply compute the right-hand side without it for the relevant range of b-values and normalize afterwards. With this PDF in hand, we can finally assign a "lensing probability" to the system as the integrated probability for impact parameters less than the critical value for multiple imaging in the SIS model—the "Einstein radius", equal to one-half the $\Delta\theta$ value given in Table 1. Summing this probability over all systems gives the estimate quoted in § 4.2 of 19 strong lenses out of 49 candidates.

REFERENCES

Abazajian, K., et al. 2003, AJ, 126, 2081
Binney, J. 2003, in IAU Symp. 220, Dark Matter in Galaxies, ed. S. Ryder, D. J. Pisano, M. Walker, & K. Freeman (San Francisco: ASP), in press; also preprint (astro-ph/0310219)
Blanton, M. R., Lupton, R. H., Maley, F. M., Young, N., Zehavi, I., & Loveday, J. 2003, AJ, 125, 2276
Brown, I. W. A., et al. 2003, MNRAS, 341, 13
Burles, S., Eisenstein, D. J., Hall, P. B., & Schlegel, D. J., for the SDSS Collab. 2000, 197th AAS Meeting #13.04
Chiba, M. 2002, ApJ, 565, 17
Crampton, D., Schade, D., Hammer, F., Matzkin, A., Lilly, S. J., & Le Fèvre, O. 2002, ApJ, 57, 86
Dalal, N., & Kochanek, C. S. 2002, ApJ, 572, 25
Doggett, J. B., & Branch, D. 1985, AJ, 90, 2303
Eisenstein, D. J., et al. 2001, AJ, 122, 2267
Eisenstein, D. J., et al. 2003, ApJ, 585, 694
Evans, N. W., & Witt, H. J. 2003, MNRAS, 345, 1351
Fassnacht, C. D., Moustakas, L. A., Casertano, S., Ferguson, H. C., Lucas, R. A., & Park, Y. 2003, ApJL, in press (astro-ph/0309060)
Freedman, W. L., et al. 2001, ApJ, 553, 47
Fukugita, M., Ichikawa, T., Gunn, J. E., Doi, M., Shimasaku, K., & Schneider, D. P. 1996, AJ, 111, 1748
Goobar, A., Mörtsell, E., Amanullah, R., & Nugent, P. 2002, A&A, 393, 25
Gunn, J. E., et al. 1998, AJ, 116, 3040
Hall, P. B., et al. 2000, AJ, 120, 1660
Hewett, P. C., Irwin, M. J., Bunclark, P., Bridgeland, M. T., & Kibblewhite, E. J. 1985, MNRAS, 213, 971
Hewett, P. C., Warren, S. J., Willis, J. P., Bland-Hawthorn, J., & Lewis, G. F. 2000, in ASP Conf. Ser. 195, Imaging the Universe in Three Dimensions, ed. W. van Breugel & J. Bland-Hawthorn (San Francisco: ASP), 94; also preprint (astro-ph/9905316)
Hippelein, H., et al. 2003, A&A, 402, 65
Hogg, D. W., Schlegel, D. J., Finkbeiner, D. P., & Gunn, J. E. 2001, AJ, 122, 2129
Hogg, D. W., Cohen, J. G., Blandford, R., & Pahre, M. A. 1998, ApJ, 504, 622
Holder, G. P., & Schechter, P. L. 2003, ApJ, 589, 688
Holz, D. E. 2001, ApJ, 556, L71
Huchra, J., Gorenstein, M., Kent, S., Shapiro, I., Smith, G., Horine, E., & Perley, R. 1985, AJ, 90, 691
Johnston, D. E., et al. 2003, AJ, 126, 2281
Kochanek, C. S. 2002a, ApJ, submitted; also preprint (astro-ph/0204043)
Kochanek, C. S. 2002b, ApJ, 578, 25
Kochanek, C. S. 2003, ApJ, 583, 49
Kochanek, C. S. 1992, ApJ, 397, 381
Kochanek, C. S., et al. 2000, ApJ, 543, 131
Kochanek, C. S., & Narayan, R. 1992, ApJ, 401, 461
Koopmans, L. V. E., & Treu, T. 2003, ApJ, 583, 606
Kotz, S., Kozubowski, T. J., & Podgórski, K. 2001, The Laplace Distribution and Generalizations: A Revisit with Applications to Communications, Economics, Engineering, and Finance (Boston: Birkhäuser)
Lupton, R., Gunn, J. E., Ivezić, Z., Knapp, G. R., Kent, S., & Yasuda, N. 2001, in ASP Conf. Ser. 238, Astronomical Data Analysis Software and Systems X, ed. F. R. Harnden, Jr., F. A. Primini, & H. E. Payne (San Francisco: Astr. Soc. Pac.), 269; also preprint (astro-ph/0101420)
Maier, C., et al. 2003, A&A, 402, 79
Mao, S., & Schneider, P. 1998, MNRAS, 295, 587
Metcalf, R. B., & Madau, P. 2001, ApJ, 563, 9
Miralda-Escudé, J., & Lehár, J. 1992, MNRAS, 259, 31P
Möller, O., Hewett, P., & Blain, A. W. 2003, MNRAS, 345, 1
Mortlock, D. J., & Webster, R. L. 2000, MNRAS, 319, 879
Mortlock, D. J., & Webster, R. L. 2001, MNRAS, 321, 629
Myers, S. T., et al. 2003, MNRAS, 341, 1
Narayan, R., & Bartelmann, M. 1996, preprint (astro-ph/9606001)
Oguri, M., & Kawano, Y. 2003, MNRAS, 338, L25
Pier, J. R., Munn, J. A., Hindsley, R. B., Hennessy, G. S., Kent, S. M., Lupton, R. H., & Ivezic, Z. 2003, AJ, 125, 1559
Porciani, C., & Madau, P. 2000, ApJ, 532, 679
Pratt, W. K. 1978, Digital Image Processing (Ney York: John Wiley & Sons)
Prugniel, P., & Soubiran, C. 2001, A&A, 369, 1048
Ratnatunga, K. U., Griffiths, R. E., & Ostrander, E. J. 1999, AJ, 117, 2010
Refsdal, S. 1964, MNRAS, 128, 307
Rusin, D., et al. 2003a, ApJ, 587, 143
Rusin, D., Kochanek, C. S., & Keeton, C. R. 2003b, ApJ, 595, 29
Schechter, P. L. 2004, in IAU Symp. 201, New Cosmological Data and the Values of the Fundamental Parameters, ed. A. N. Lasenby & A. Wilkinson (San Francisco: ASP), in press; also preprint (astro-ph/0009048)
Schechter, P. L., & Wambsganss, J. 2002, ApJ, 580, 685
Schechter, P. L., Burley, G. S., Hull, C. L., Johns, M., Martin, H. M., Schaller, S., Schectman, S. A., & West, S. C. 2003, in Proc. SPIE 4837, Large Ground-Based Telescopes, ed. J. M. Oschmann & L. M. Stepp (SPIE), 619; also preprint (astro-ph/0207250)
Schlegel, D. J., Finkbeiner, D. P., & Davis, M. 1998, ApJ, 500, 525
Sluse, D., et al. 2003, A&A, 406, L43
Smith, J. A., et al. 2002, AJ, 123, 2121
Spergel, D. N., et al. 2003, ApJS, 148, 175
Stoughton, C., et al. 2002, AJ, 123, 485
Strauss, M. A., et al. 2002, AJ, 124, 1810
Treu, T., & Koopmans, L. V. E. 2002, ApJ, 575, 87
Turner, E. L., Ostriker, J. P., & Gott, J. R. 1984, ApJ, 284, 1
Warren, S. J., Hewett, P. C., Lewis, G. F., Møller, P., Iovino, A., & Shaver, P. A. 1996, MNRAS, 278, 139
Warren, S. J., Iovino, A., Hewett, P. C., & Shaver, P. A. 1998, MNRAS, 299, 1215
Warren, S. J., Lewis, G. F., Hewett, P. C., Møller, P., Shaver, P. A., & Iovino, A. 1999, A&A, 343, L35
Willis, J. P., Hewett, P. C., Warren, S. J., & Lewis, G. F. 2000, in Proceedings of the XXth Moriond Meeting: Cosmological Physics with Gravitational Lensing, ed. J. Tran Thanh Van, Y. Mellier, & M. Moniez (Les Ulis: EDP Sciences); also preprint (astro-ph/0008068)
Witt, H. J, Mao, S., & Schechter, P. L. 195, ApJ, 443, 18
York, D., et al. 2000, AJ, 120, 1579